Improvement in the Imaging Performance of Atomic Force Microscopy: a Survey

M. S. Rana, *Member, IEEE*, H. R. Pota, *Member, IEEE*, and I. R. Petersen, *Fellow, IEEE*

***Abstract*—Nanotechnology is the branch of science which deals with the manipulation of matters at an extremely high resolution down to the atomic level. In recent years atomic force microscopy (AFM) has proven to be extremely versatile as an investigative tool in this field. The imaging performance of AFMs is hindered by: (i) the complex behavior of piezo materials, such as vibrations due to the lightly damped low-frequency resonant modes, inherent hysteresis and creep nonlinearities; (ii) the cross-coupling effect caused by the piezoelectric tube scanner (PTS); (iii) the limited bandwidth of the probe; (iv) the limitations of the conventional raster scanning method using a triangular reference signal; (v) the limited bandwidth of the proportional-integral (PI) controllers used in AFMs; (vi) the offset, noise, and limited sensitivity of position sensors and photodetector; and (vii) limited sampling rate of AFM's measurement unit. Due to these limitations, an AFM has a high spatial but low temporal resolution, i.e., its imaging is slow, e.g., an image frame of a living cell takes up to 120 s, which means that rapid biological processes that occur in seconds cannot be studied using commercially available AFMs. There is a need, to perform fast scans using an AFM with nanoscale accuracy. This paper presents a survey of the literature, presents an overview of a few emerging innovative solutions in AFM imaging, and finally proposes future research directions.**

***Note to Practitioners*→ An atomic force microscope (AFM) is a scientific instrument capable of investigating, controlling, and manipulating matter on a nanoscale. It is a fundamental part of research in the field of nanotechnology because of its capability to obtain 3D images of specimens in the areas of life sciences and materials science. However, the imaging performances of currently available AFMs are restricted by some limitations which, during the last two decades, several works have attempted to overcome in order to meet present demands. This article presents an overview of developments in AFM imaging, emphasizing the key roles of: the modeling, control techniques, and mechanical structural designs of an AFM's piezoelectric tube scanner (PTS) and probe; different scanning methods; and sensor noise compensation techniques.**

***Index Terms*—Nanotechnology, scanning probe microscopy, atomic force microscopy, piezoelectric tube scanner, position sensor, resonant mode, creep, hysteresis, cross-coupling.**

I. Introduction

SCANNING probe microscopy (SPM) opens a new window to the nano-world. It is a widely used tool in nano measurement techniques. It is one of the key techniques in nanotechnology that relies heavily on nanopositioning. SPM uses a physical probe to scan back-and-forth over the surface of a sample. SPMs are different from optical microscopes because the user does not "see" the surface directly. Instead, these tools "feel" the surface and create an image. The reason for calling them SPMs is they use a probe for investigating and manipulating matter.

The first SPM, the scanning tunneling microscope (STM), was invented in 1981 by the Swiss scientists Gerd Binnig and Heinrich Rohrer [1]–[3] who were awarded the Nobel Prize in Physics in 1986. An STM is capable of directly obtaining three-dimensional (3D) images of solid surfaces. However, as it is only used to measure the topography of surfaces which are electrically conductive, its use for surfaces which are non-conductive is limited. To overcome this limitation, several SPMs with similar working principles were invented within a short period of time, e.g., the scanning near-field optical microscope (SNOM) [4], scanning thermal microscope [5], atomic force microscope (AFM) [6], magnetic force microscope (MFM) [7], scanning chemical potential microscope (SCPM) [8], electric force microscope (EFM) [9], scanning ion conductance microscope (SICM) [10], and scanning capacitance microscope (SCM) [11].

Currently, of all the SPMs, the AFM is playing the most dominant role in the field of nanotechnology [13]–[16]. Although present AFMs (Fig. 1(b) [12]) differ in many ways from that invented by Gerd Binnig *et al.* in the mid-1980s (Fig. 1(a) [3]), its basic principles remain the same. It has the capability to generate 3D images of material surfaces at an extremely high resolution down to the atomic level (10^{-10} m) [6]. It enables precise control, manipulation, and interrogation of matter at the nanoscale level [17]. The invention of the AFM has opened up a new era in the field of nanotechnology to study non-conductive sample surfaces. The AFM can be used to measure the topography of any surface, whether it is electrically conductive or insulating. Recently, the use of AFM probes has been extended to enable the mapping of a wide range of mechanical, electrical, chemical, biological, and physical interactions [3], [18]–[21].

Conventional AFMs take minutes to acquire an image and, since many biological and chemical processes occur in less than a minute, much could to be gained by a faster scan rate. Existing AFMs have the following limitations which prevent it from achieving high scanning speeds: (i) the complex behavior of piezo materials, such as vibrations due to the lightly damped low-frequency resonant modes, inherent hysteresis and creep nonlinearities; (ii) the cross-coupling effect caused by the PTS; (iii) the limited bandwidth of the probe; (iv) the limitations of the conventional raster scanning method using a triangular

M. S. Rana is with the Department of Electrical and Electronic Engineering, Rajshahi University of Engineering and Technology (RUET), Rajshahi-6204, Bangladesh and, H. R. Pota and I. R. Petersen are with the School of Engineering and Information Technology, the University of New South Wales, Canberra, ACT 2600, Australia (e-mail: sohel.unsw@gmail.com; h.pota@adfa.edu.au; i.petersen@adfa.edu.au).

This work has supported by the Australian Research Council (ARC) under the Grant of FL11010002 and the UNSW Canberra under the Rector Fellowship.

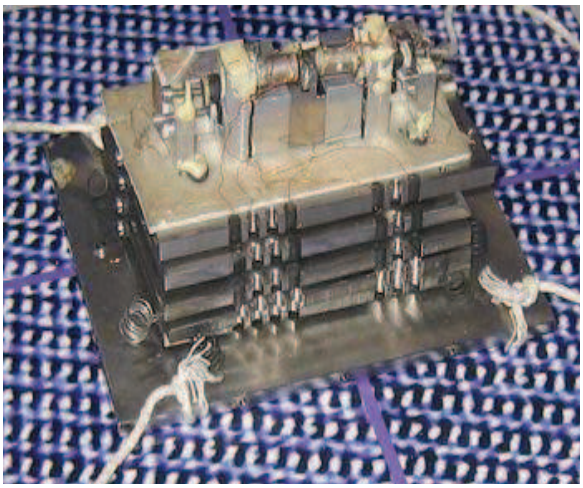

(a)

(b)

Fig. 1. Development of AFM: (a) the first AFM (invented by G. Binnig, C. F. Quate, and Ch. Gerber) [3] and (b) a modern NT-MDT Ntegra AFM [12].

reference signal; (v) the limited bandwidth of the proportional-integral (PI) controllers used in AFMs; (vi) the offset, noise, and limited sensitivity of position sensors and photodetector; and (vii) limited sampling rate of AFM's measurement unit.

This paper reviews the problems associated with high-speed AFM imaging and presents existing solutions. It is organized as follows. Section II presents a brief description about AFM basics; Section III presents the factors of the PTS which limit the scanning speed of AFM; Section IV the problems with the probe; Section V the limitations of the conventional scanning method in AFM imaging; Section VI the limitations of the existing controllers; Section VII the limitations of the AFM's position sensor; Section VIII the limitations of the AFM's photodetector; Section IX the limitations of the AFM's measurement unit; Section X existing solutions to the limitations of AFM imaging; and, Section XI future research directions and conclusions.

II. AFM Basics

In recent years, of all the available microscopy techniques, AFM has proven to be extremely versatile as an investigative tool in the field of nanotechnology. A standard layout of an AFM is shown in Fig. 2. Its basic components include a micro-cantilever (probe) with a sharp tip on its free end, a positioning unit, i.e., piezoelectric tube scanner (PTS), a laser source, and a laser photodetector.

The operation of an AFM is based upon the principle of sensing the forces between a sharp tip and the surface to be investigated. The forces can be attractive or repulsive depending on the operating modes [see Fig. 3]. When the tip is brought close to the sample, a number of forces may operate between it and the sample [22], as shown in Fig. 3(a). Typically, the forces contributing most to the movement of the AFM cantilever are the van der Waals and short-range repulsive interactions, and adhesion and capillary forces. Figure 3(b) shows a complete picture of the different types of forces acting between the tip and a sample. The forces between the tip and sample cause a deflection of the cantilever which is measured by a laser reflected off the cantilever into a position-sensitive photodiode (PSPD). As the photodiode collects more light, it creates an output signal that is processed and provides information about the vertical bending of the cantilever which is then sent to the feedback controller which keeps the force constant by controlling the expansion of the Z-piezo of the PTS. According to the controller's information, the scanner maintains the height of the probe as it moves across the surface and the variations in height can then be used to produce a 3D topographical representation of the sample.

A. Operating Modes

An AFM is usually described as operating in one of the following three modes depending on the nature of the tip motion [3]:

- contact mode, also called static mode ($<$0.5 nm probe-surface separation)
- tapping mode, also called intermittent contact, AC-mode, or vibrating mode, or, after the detection mechanism, amplitude modulation (AM) AFM (0.5–2 nm probe-surface separation) mode
- non-contact mode, or, again after the detection mechanism, frequency modulation (FM) AFM (0.1–10 nm probe-surface separation) mode

A brief description of these three modes is given below.

1) Contact Mode: This is the most common mode in which the AFM tip makes soft 'physical contact' with the surface of the sample and the deflection of the cantilever Δx is proportional to the force acting on the tip via Hooks law ($F = -k\Delta x$, where k is the spring constant of the cantilever).

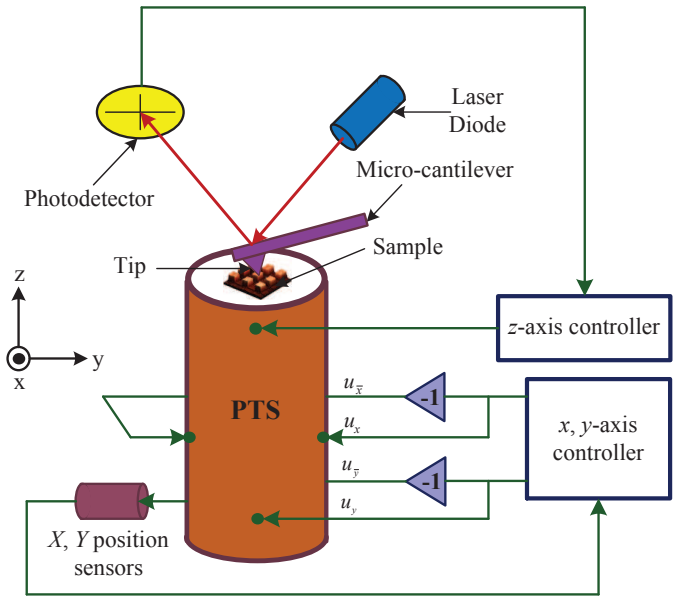

Fig. 2. Schematic view of an AFM.

In this mode, the tip scans either at a constant small height above the surface or under conditions of a constant force. For the former, the height of the tip is fixed whereas, for the latter, the deflection of the cantilever is fixed and the motion of the scanner in the z-direction recorded. By using this mode, 'atomic resolution' images can be obtained.

The force acting on this mode is a repulsive one in the order of 10^{-9} N. This mode is used when imaging materials that are not adversely affected by being in sheer with a sharp tip which is generally made of silicon nitride. For contact-mode AFM imaging, it is necessary to use a cantilever which is soft enough to be deflected by very small forces but has a sufficiently high resonance frequency so that it is not susceptible to vibrational instabilities. The tip-sample position in contact mode operation of the AFM is shown in Fig. 4(a).

The advantages and disadvantages of the contact mode operation of the AFM are as follows.
Advantages:

- high scanning speeds;
- possible 'atomic resolution'; and
- easier scanning of rough samples with extreme changes in vertical topography.

Disadvantages:

- lateral forces can distort the image;
- capillary forces from a fluid layer can cause large forces normal to the tip-sample interaction; and
- a combination of these forces reduces spatial resolution and can cause damage to soft samples.

2) Tapping Mode: The tapping mode is also called semi-contact mode. This is an important mode in AFM imaging because it enables high-resolution imaging of a sample surface that is easily damaged, loosely held to its substrate or difficult to image by other AFM imaging techniques. In this mode, the cantilever is oscillates at its resonance frequency by alternately placing its tip in contact with the surface to provide high resolution. Then the tip is lifted off surface to avoid dragging the tip across the sample. The oscillation of the cantilever in tapping mode is achieved using a piezoelectric crystal at the base of the cantilever. When the piezoelectric crystal moves, the cantilever oscillates. In tapping mode, the cantilever oscillates at or slightly below its resonance frequency with the amplitude of oscillation typically ranging from 20 to 100 nm [23]. The oscillation amplitude of the tip is measured by the optical detector and provides an input to the controller electronics that maintains a constant height or force. A feedback circuit adjusts the tip-sample separation to maintain a constant amplitude of oscillation, i.e., the amplitude's set-point. Tapping mode overcomes problems associated with friction, adhesion, and other difficulties. The tip-sample position in tapping mode operation of the AFM is shown in Fig. 4(b).

The advantages and disadvantages of an AFM's tapping mode operation are as follows.
Advantages:

- higher lateral resolution;
- lower forces and less damage to soft samples in air; and
- almost no lateral forces.

Disadvantage:

- slower scanning speed than the contact mode.

3) Non-contact Mode: In this mode, the cantilever is brought into close proximity (within a few nanometers) of the sample, the probe vibrates at a particular frequency, and changes in the frequency are used to detect the surface structure of the sample. The amplitude of the oscillation is slightly less than the nominal tip to surface distance of less than 10 nm, there is interaction between the tip and surface, but this is not considered as a contact. The attractive van der Waals force acts between the tip and the sample but it is substantially weaker than the forces in contact mode. The non-contact mode is used in situations in which contact with the tip might alter the sample in subtle ways. In it, the tip hovers between 50 $\mathring{A}$ and 150 $\mathring{A}$ above the sample surface. Normally, the cantilever used in this mode has higher stiffness and a high spring constant in the order of 20-100 N/m to prevent it from sticking to the sample surface. The forces between the tip and sample are quite low, in the order of 10^{-12} N. The tip-sample position in non-contact mode operation of the AFM is shown in Fig. 4(c).

The advantages and disadvantages of the non-contact mode of operation of the AFM are as follows.
Advantage:

- as a low force is exerted on the sample surface, no damage is caused to soft samples.

Disadvantages:

- lower lateral resolution, limited by tip-sample separation;
- slower scanning speed to avoid contact with the fluid layer; and
- usually only applicable for extremely hydrophobic samples with a minimal fluid layer.

Table I presents a summary of the main characteristics of the three modes.

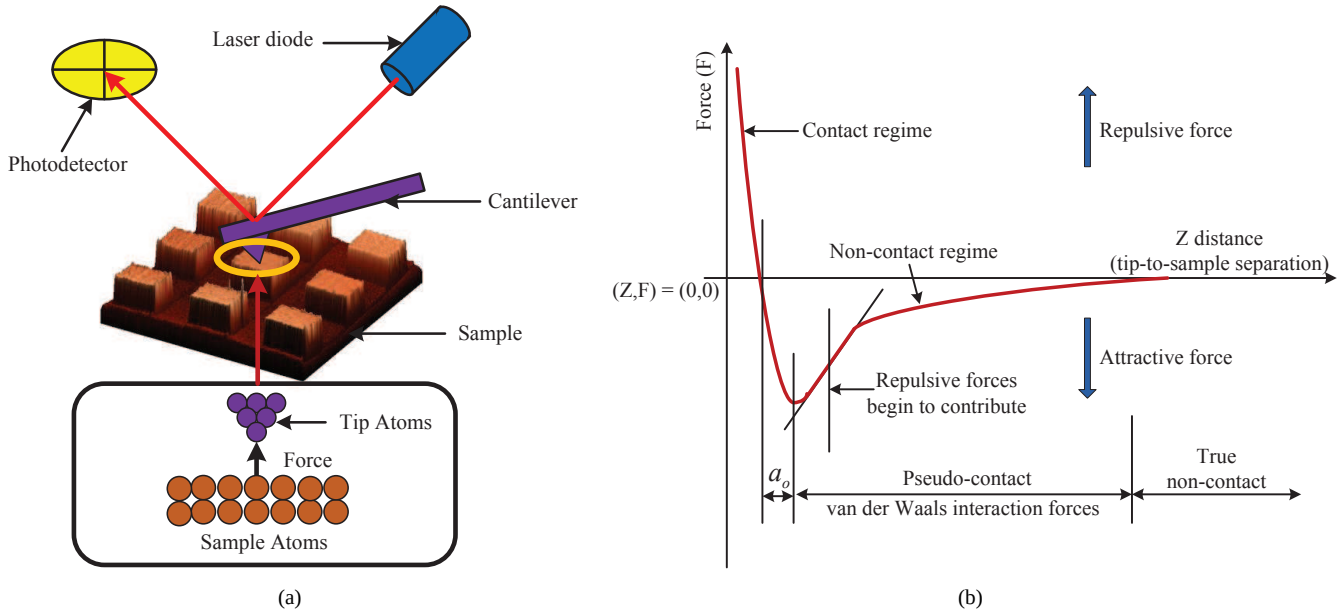

Fig. 3. (a) interaction forces between a sharp tip and a sample in an AFM and (b) force vs. distance curve at different operating modes of an AFM.

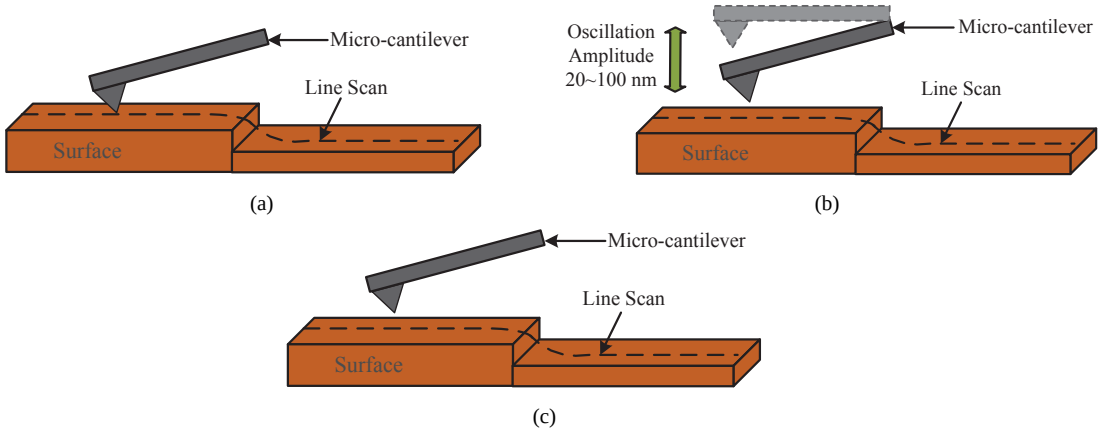

Fig. 4. Operating modes of the AFM: (a) contact mode, (b) tapping mode, and (c) non-contact mode.

III. Limiting Factors of a PTS

Piezoelectric transducers have become ubiquitous in applications requiring precision motion and force control, e.g., positioning systems [24], fuel injection valves [25], laser beam manipulation [26], machine tools [27], surgical tools [28], SPMs [29], pumps [30], micro-motors [31], and vibration control systems [32]. The PTS is a special type of piezoelectric transducer.

In most applications of nanotechnology, speed and precision are important requirements for obtaining good topographical maps of material surfaces using AFMs, many of which use PTSs for scanning and positioning at nanometric resolutions. A PTS is the most useful actuator in nanopositioning applications, e.g., microscopes, and is made of ceramic lead zirconate and titanate (PZT). It consists of a tube of radially poled piezoelectric material, four external electrodes, and a grounded internal electrode as shown in Fig. 5. Its external electrodes are divided into four parts: $+X$ and $-X$ form the X–electrode; and $+Y$ and $-Y$ the Y–electrode pairs, while the internal Z–electrode is continuous. The reason for using such a configuration is that it halves the input voltage requirements and results in more power being provided to the electrodes. The PTSs AFM scanners are of two types: (i) scan-by-sample scanner and (ii) scan-by-head scanner, both of which are used in various nanopositioning applications. A PTS (NT-MDT z50313cl) mounted with capacitive sensors is shown in Fig. 6.

The main features of the PTS are that it can generate a large force in a range of temperatures, is generally free of wear and tear, has a fast response time, requires little maintenance, and is not affected by magnetic fields. In spite of its many useful properties, there are some challenges associated with its use for precision positioning. It suffers from various intrinsic problems that degrade its positioning performance, such as: (i) resonant modes due to its mechanical structure [33]–[37]; (ii) nonlinear behavior due to hysteresis and creep [38]–[43]; and (iii) the cross-coupling effect between its axes (in 3D positioning systems like AFMs) [44]–[46]. Because of these

TABLE I
COMPARISON OF DIFFERENT OPERATING MODES OF AN AFM

Characteristics	Operating mode		
	Contact mode	Tapping mode	Non-contact mode
Tip loading force	low → high	low	low
Contact with sample surface	yes	periodical	no
Manipulation of sample	yes	yes	no
Contamination of AFM tip	yes	yes	no

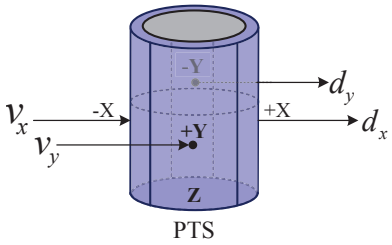

Fig. 5. I/O diagram of the AFM PTS.

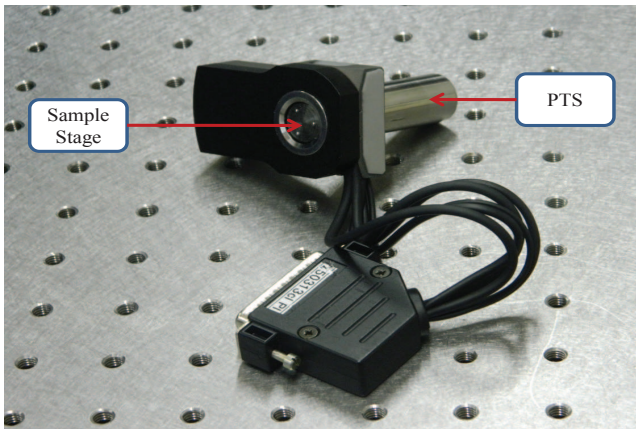

Fig. 6. The PTS with internally mounted capacitive position sensors. Adapted from [47].

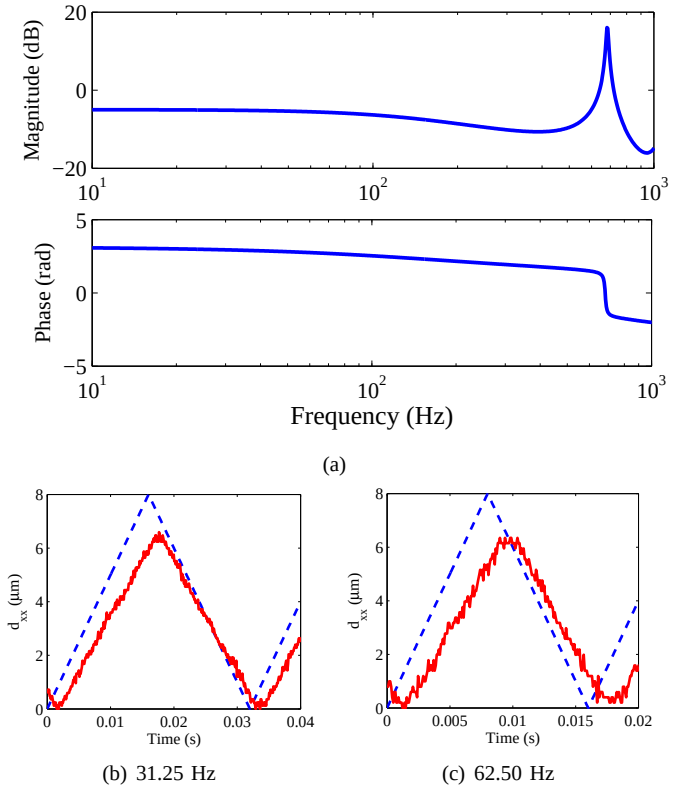

Fig. 7. Vibration effects in a PTS system. (a) frequency response and; effects of scan-induced vibrations on the PTS tracking performance in open-loop at (b) 31.25 Hz and (c) 62.50 Hz scanning speeds [reference signal (dashed line - -) and output signal (solid line –)].

limitations, AFMs suffer in terms of tracking accuracy which creates significant effects in scanned images. These issues are further elaborated in the following subsections.

A. Vibrations Effect

The performance of an AFM in high-speed imaging is limited by a number of factors. The most exigent issue that causes problems for the high-speed nanopositioning of a PTS is its low mechanical resonance frequency to which its bandwidth is limited. Due to the resonant nature of the PTS, its resulting sensor displacement may be oscillatory at high scanning speeds which causes successive erosion of the scanner and degrades its performance. Due to this limitation, vibration is created in an AFM's scanned images which has become a major concern of researchers.

The currently available AFM's scanning speed is limited to less than $0.01 f_r$, where f_r is the frequency of the resonant mode of the PTS [48]. Since, in most AFMs, f_r is approximately 1 kHz, this means that the scanning speed is limited to about 10 Hz.

Figure 7(a) shows a frequency response of a PTS in which it can be seen that, at around 700 Hz, the system has an uncontrolled resonant mode. In Figs. 7(b) and (c), the open-loop tracking performance at 31.25 Hz and 62.50 Hz, respectively, are presented. Due to the uncontrolled tube resonance, the scanner displacements become distorted since, the characteristic time of scan and PTS resonance become comparable, and beats from the latter couple in with the former. Therefore, the scanning results in images affected by vibrations that are not triggered and jitter between different lines within the same frame shown in Figs. 8(a) and (b).

B. Nonlinearity Effects

There are two major nonlinearity effects which exist in piezoelectric materials, i.e., hysteresis and creep [39], [49], as explained briefly in the following.

1) Hysteresis Effect: PTSs are preferred in designs of high-speed nanopositioning systems because they have a compact

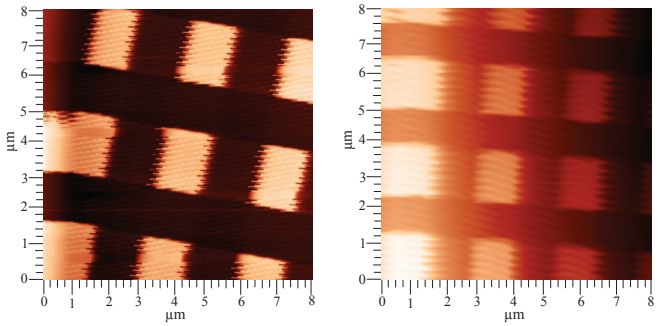

(a) 31.25 Hz (b) 62.50 Hz

Fig. 8. Effects of scan-induced vibrations in the PTS on open-loop scanned AFM images at 31.25 Hz and 62.50 Hz scanning speeds, respectively.

geometry and can generate high forces over a large bandwidth. However, the relationship between the applied voltage and output displacement of these scanners is not linear. When an external voltage is applied in a piezo, it elongates because of the material's behavior but, when the voltage is released, it follows another path and creates a loop. This loop is known as a hysteresis loop. This deviation from linearity depends on the scanner's geometry and material, and cannot be fully predicted but happens because the piezo is like a capacitor and stores energy. It is a memory effect [50] that occurs in such phenomena as plasticity, friction, ferromagnetism, and superconductivity. It depends not only on the input at the present time but also on the operational history of the system considered. It is evident that the effects of hysteresis are significant in large AFM images.

An electromechanical model formulated for a piezoelectric actuator (PEA) to describe the hysteresis effect is given by as [51], [52]:

$$\dot{q} = \alpha|\dot{U_h}|(aU_h - q) + b\dot{U_h}; \tag{1}$$

where $\alpha > 0$, $a > 0$, and $b > 0$ are constants which determine the size and shape of the hysteresis nonlinearity. If α is small, the system can be considered approximately linear.

As piezoelectric materials are ferroelectric materials, they exhibit hysteretic behavior when driven by a voltage source which increases as the amplitude or frequency of the applied voltage signal increases. On the other hand, in low-range scans (i.e., when actuating a PTS with voltage signals of low amplitudes), hysteresis can be ignored [33]. Due to this effect, a PTS gives rise to problems of inaccuracy or oscillation and even leads to the degradation of stability in both open-loop and closed-loop controls. Moreover, the dynamics of the hysteresis in different axes are usually unknown. Therefore, it is a challenging task to design a control system with high performance for a PTS subject to the hysteresis phenomenon.

Figure 9(a) illustrates the displacement in the x–axis of a PTS when driven by a triangular wave voltage signal in the open-loop case. In Fig. 9(b), the scanner's displacement is plotted against the reference signal to form a hysteresis curve. Figure 9(c) illustrates a 31.25 Hz AFM scanned image which is suffering badly from hysteresis effects in which it can be observed that, due to the presence of a hysteresis nonlinearity,

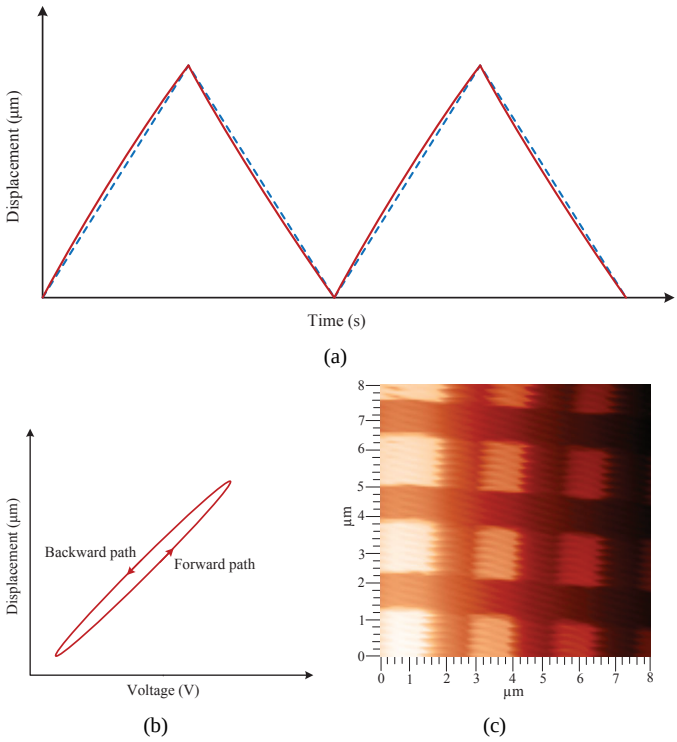

Fig. 9. Effect of hysteresis on a PTS when driven by a voltage source: (a) measured scanner displacement (solid line –) and reference signal (dashed line - -); (b) hysteresis curve illustrating the relationship between the reference input signal and the scanner's displacement; and (c) scanned AFM image suffering from the hysteresis effect.

its stretches one end of the scan and compresses the other end.

2) Creep Effect: An unwanted change in displacement over time is called creep, which is another nonlinearity that occurs with low frequency signals and can be severe in the slow operation of an AFM. When the applied voltage signal goes through an abrupt change, such as a step change, the PTS experiences two stages of dimensional change. In the first stage, it undergoes an instantaneous dimensional change within less than a millisecond; and, in the second stage, after the input voltage change is completed; it continues to undergo a relatively small dimensional change in the same direction but over a much longer time. This slow dimensional change behavior in the second stage is known as creep.

Creep is a function of the time and input voltage and is described in [53] as:

$$y(t) = y_o\{1 + \gamma log(\frac{t}{t_o})\}; \tag{2}$$

where t_o represents the time at which the creep effect is apparent, y_o is the value of the actuator displacement at time t_o, and the creep rate, γ, is a fixed value that can be identified by observing the step response of the actuator.

In mechanics, creep is a rate-dependent deformation of a material subjected to a constant load or stress and, similarly, in a piezoelectric material, is a rate-dependent deformation due to a constant electrical field [54]. Creep manifests itself when the remnant polarization slowly increases after the onset of a constant field. In particular, creep has two adverse effects

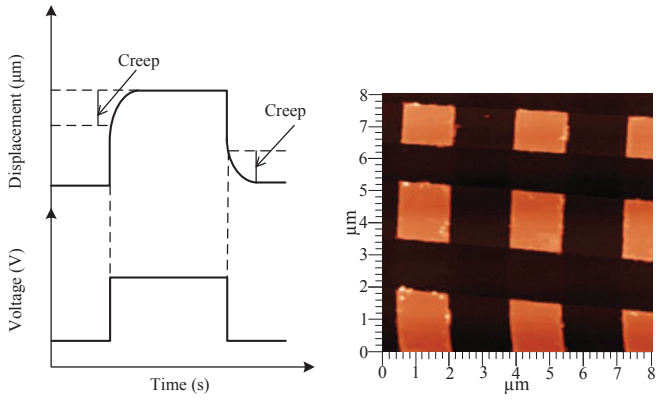

Fig. 10. Effect of creep on the PTS when driven by voltage source: (a) creep effect and (b) scanned AFM image suffering from the creep effect.

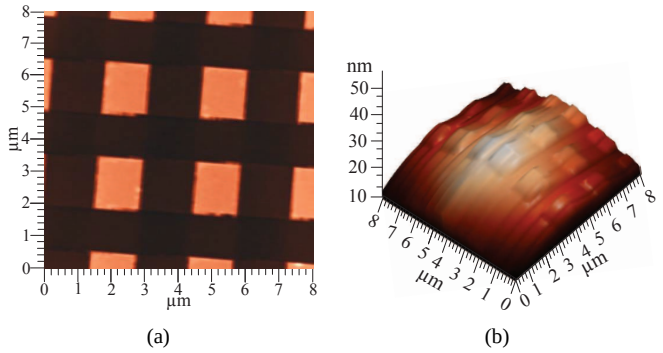

Fig. 11. Effect of cross-coupling on scanned AFM image: (a) X–to–Y cross-coupling motion (b) XY–to–Z cross-coupling motion.

in AFMs: (i) the vertical position of the tip will creep after it approaches the sample and (ii) it exacerbates the effect of hysteresis at the turning point of the scanning trajectory [55].

In Fig. 10(a), to illustrate the creep effect, a square wave is applied to the PTS to record its displacement and it is shown that its edges become curved. Figure 10(b) shows a $8\ \mu$m $\times$ $8\ \mu$m scanned AFM image, the vertical edges of which roll-off because of the creep effect.

C. Cross-coupling Effect

Movement in the x– or y–axis direction produces spurious motion in the z–axis direction which is called the cross-coupling effect and is one of the most significant causes of the poor performance of scanners in nanopositioning. It generally exists in piezoscanners used for 3D (x–y–z axes) nanopositioning in applications such as the AFM and produces a bowl-shaped image of a flat surface. Its sources include the tensor nature of the strain fields, the fact that the electrical field is not uniform across the piezo tube, the existence of "cross talk" among the X–, Y–, and Z–electrodes, and the fact that, by nature of its geometry, the piezo tube scans in an arc not a plane. Such x/y–to–z cross-coupling becomes pronounced when the scanning is over a large range or at a high-speed due to the excitation of the mechanical resonances of the scanner.

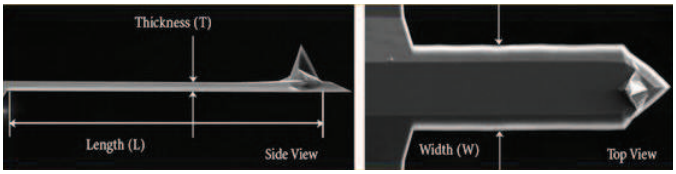

Fig. 12. A CGS01 micro-cantilever. Adapted from [3].

In AFM applications, when the position errors caused by coupling are large, large imaging distortions or damage of the cantilever probe or sample can result. Due to the cross-coupling effect, the PTS's trajectory becomes distorted and loses precise positioning when operated at high frequencies and wide scanning ranges. Due to the presence of the cross-coupling effect, the signal applied to the X–axis will corrugate the traced trajectory in the X–Y plane. The cross-coupling effect not only corrugates scans but introduces artifacts to the image which can be mistakenly identified as surface roughness [39], [49]. Although proportional-integral (PI) controllers have been used to reduce the effects of hysteresis and creep with considerable success, they are often not designed to deal with the cross-coupling issue. Fig. 11(a) shows a $8\ \mu$m $\times$ $8\ \mu$m scanned AFM image which becomes tilted because of the cross-coupling effect between the lateral axes (X and Y). Due to cross-coupling between XY–to–Z, the scanned AFM image becomes bowl-shaped, as shown in Fig. 11(b).

IV. Problems with AFM Probe

Surface sensing in the AFM is performed using a special probe usually made of an elastic cantilever with a sharp tip at the end as shown in Fig. 12. It is one of the major parts of the AFM. Such probes are produced by photolithography and the etching of silicon where SiO_2 or Si_3N_4 layers are deposited onto a silicon wafer. One end of the cantilever is firmly fixed on the silicon base-holder, and the tip is located close to the free end of the cantilever. There are two important properties of the cantilever, one is resonance frequency, and the other is spring constant. The resonance frequency should be high, in order to get low coupling of external vibrations to the cantilever and to get a high imaging speed. The lower spring constant is required for the higher sensitivity. The cantilever's resonance frequency is important during AFM operation in the oscillating modes and its oscillation frequencies are determined by [56]:

$$f_r = \frac{\lambda_i}{2\pi l^2}\sqrt{\frac{EJ_c}{\rho S}} \tag{3}$$

where l is the cantilever length, E is the Young's modulus, J_c is the inertia moment of the cantilever cross-section, ρ is the material density, S is the cross-section, and λ is a numerical coefficient. The spring constant for a cantilever shaped like a rectangular bar of width w is [57]:

$$K = \frac{Ewd^3}{4l^3}. \tag{4}$$

Tapping is the most prevalent AFM imaging mode as it greatly reduces sample damage and distortion compared with

alternative modes of operation [58]. However, in this mode, an AFM has a relatively slower scanning speed than alternative imaging modes. The maximum obtainable scanning speed is limited by the bandwidth of the z–axis feedback loop which is inversely proportional to the quality factor (Q) of the cantilever, i.e., $B = \pi f_r/Q$, where f_r is the resonance frequency of the cantilever [59]. To achieve a high scanning speed, Q needs to be reduced. Again, the maximum achievable imaging speed of an AFM is limited by the bandwidth of the cantilever. The exact relationship between the cantilever's resonance frequency and the cantilever-imposed limit of the tip-sample measurement bandwidth depends strongly on the mode of operation and detection method but is proportional to the resonance frequency.

V. Problems with Conventional Scanning Methods

Currently, conventional AFMs use the raster scanning technique which is a key limitation for high-speed imaging. In raster pattern scanning, as shown in Fig. 13(c), the PTS moves along the x–axis (fast axis) in the forward and reverse directions (line scan), and then along the y–axis (slow axis) in small steps to reach the next scan line. These movements are accomplished by applying a triangular wave signal to the x–axis and a slowly increasing staircase signal to the y–axis of the scanner, as illustrated in Figs. 13(a) and (b), respectively. The triangular signal contains odd harmonics of the fundamental frequency which excite the resonance of the PTS. The amplitudes of these signal harmonics attenuate as $1/n^2$, with n the harmonic number. If a fast triangular waveform is applied to the scanner, it inevitably excites the scanner's mechanical resonance, causing the scanner to vibrate and trace a distorted triangular waveform which can significantly distort the generated AFM image. To avoid this problem, the scanning speed of an AFM is often limited to 1% [60], [61] of its PTS's first resonance frequency. For most AFMs, the resonance frequency is approximately 1 kHz which means that the scanning speed is limited to about 10 Hz.

VI. Limited Bandwidth of the Controller

To achieve high-speed imaging, it is necessary to increase an AFMs scanning speed by improving the closed-loop bandwidth of the overall system. Most commercial available AFMs use an integral or proportional-integral (PI) controller in the axes of the PTS because of their simplicity, robustness to modeling error, and ease of implementation. The bandwidth of such integral controllers is limited due to the highly resonant modes of the PTS. The maximum closed-loop bandwidth that can be achieved with an integral controller for the PTS is less than $2\pi f_r \xi$, where ξ is the damping constant of the PTS. The damping constant of the PTS is usually very low, in the order of 0.01, which means that the maximum closed-loop bandwidth that can be achieved by using an integral controller is less than 2% of the first resonance frequency. Therefore, a current major challenge is to achieve nanopositioning of an AFM with a high bandwidth [32].

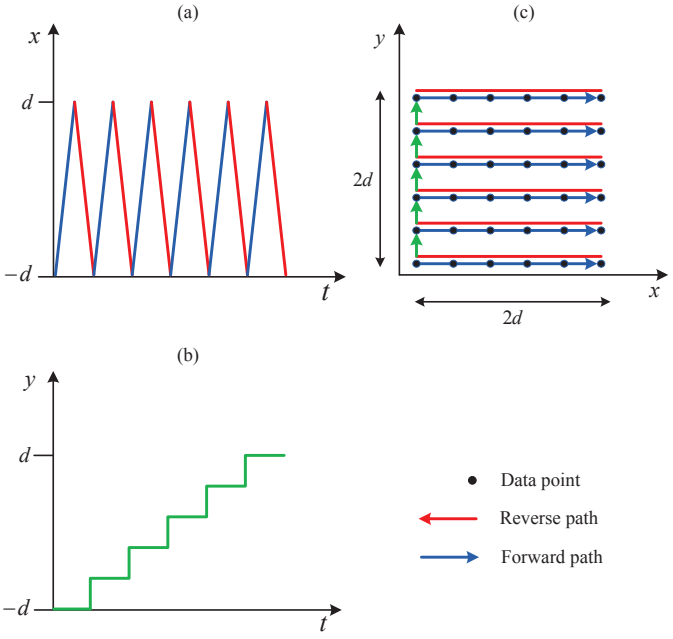

Fig. 13. In order to force the scanner to trace a raster pattern (c) in the x–y plane, a triangular signal (a) is applied to the fast-axis, and a staircase signal (b) to the slow-axis.

VII. Problems with the Position Sensors

Position sensors with nanometer resolution are a key component of precision imaging machines and nanofabrication processes. They are designed to produce an output that is directly proportional to the measured position. However, in reality, all position sensors have an offset, nonlinear response, and limited sensitivity. These effects must be compensated to achieve positioning accuracy. In nanopositioning applications, different types of position sensors like capacitive, inductive, piezoresistive, electrothermal, linear variable displacement transformer (LVDT), optical, eddy current, magnetoresistive, etc., are used to measure the displacement. Details of these sensors are presented in [62].

Although position sensors were not incorporated in the first generation AFMs, they are successfully being built into new commercially available AFMs. In AFM nanopositioning, capacitive and inductive sensors are commonly used because of their high-resolution measurement capability. However, they have self-noise which degrades the performance of the feedback loop and results in adverse effects on the AFM imaging performance. An estimate of the RMS positioning noise can be found by using the following equation [32]:

$$\text{RMS noise} = \sqrt{2 \times \text{bandwidth}} \times \text{noise density} \qquad (5)$$

To appreciate this, consider a displacement sensor that has a root-mean-square (RMS) noise of 20 pm/$\sqrt{\text{Hz}}$ which is typical for most capacitive and inductive displacement sensors [43]. If the sensor is operated over a bandwidth of, say 10 kHz, its RMS noise will be 2.8 nm, which makes it impossible to achieve subnanometer positioning accuracy. This limitation can be overcome by reducing the bandwidth, e.g., for 100 Hz scanning speed the noise level is reduced to 2 Å, about the radius of an atom. Thus, the positioning accuracy achievable by

a feedback controller can be significantly improved. However, this would also limit the operating bandwidth of the feedback controller, resulting in very slow closed-loop operation. Such a severe closed-loop bandwidth limitation would come at the additional cost of making the closed-loop system sensitive to vibration, noise, and other disturbances.

VIII. Problems With The Photodetector

Position sensitive photodetector (PSPD) plays an important role in the AFM circuitry. The photodetector capable of converting light either current or voltage, depending upon the mode of operation. When a laser beam being reflected off the back of the cantilever in to a PSPD that records changes in the laser PSPD position as a voltage relative to the angular cantilever deflection. The output of the photodetector is provided to a computer for processing of the data for providing a topographical image of the surface with atomic resolution. The PSPD technique is used widely because of its ease force measurement procedure. However there are a number of complications and disadvantages associated with this measurement, such as, limited sensitivity [63].

IX. Limited Sampling Rate Of The Measurement Unit

Sampling rate is directly related to the image resolution. If the sampling rate is increased (up-sampling), the image resolution is increased. Similarly, down-sampling decreases image resolution. The sampling rate of the measurement unit is one of the limitations in the AFM system. This effect is more severe in the vertical direction than the lateral direction because of its faster dynamics. For faster control in the vertical direction, a more sophisticated feedback controller would have to be implemented on a field-programmable-gate-array (FPGA), since standard digital signal processors (DSP) are not able to handle the amount of data required to operate the AFM system in real-time [64]. If a feedback controller is to include a 300 kHz resonance in the model, then a typical rule-of-thumb sample rate of 10–20 times the highest dynamics of interest would imply a 3–6 MHz sample rate for the control system [65]. Obviously, such a high sample rate puts severe constraints on the signal processing system, not just in accomplishing the needed processing between samples, but also in minimizing the latency of the computations, signal conditioning, and data conversion.

X. Existing Solutions

To overcome the above limitations, three general approaches have been adopted by various researchers. The first implements different control techniques, the second changes the scanning pattern and, the third changes the mechanical structure of the scanner stage and the cantilever head.

A. Different Control Techniques

The conventional PI controller commonly used in AFM systems is not capable of providing high scanning accuracy or robustness against nonlinear effects and parameter variations [52], [66]. To address the challenges in high-speed AFM imaging, many control efforts have been made over the last decade [67], [68]. Roughly speaking, the existing control techniques can be classified into the following three categories: (i) feedback control, (ii) feedforward control, and (iii) charge control.

1) Compensation of Vibration Effect: The vibration effect can be compensated by proper damping of the resonant modes. Research on this issue has been conducted by several authors [32], [47], [68]–[70]. In [68], the signal transformation method shown in Fig. 14 is implemented to track a triangular reference signal. However, its performance suffers for high frequency scanning because it cannot achieve a great deal of damping of the resonant modes. A recent solution to this drawback is impulsive state multiplication (ISM) control which is suitable for piece-wise linear (affine) references such as triangular waveforms [71]. An alternative solution that leads to a better transient performance in signal transformation called the initialized signal transformation approach (ISTA) is proposed in [72].

Several feedback controllers have been applied to damp the resonant mode of a PTS, such as positive position feedback (PPF) control in [61]. The PPF controller is a low-pass filter with a fast roll-off at high frequencies and high gain at low frequencies. However, due to its low-pass nature, it suffers from the problem of a low gain and phase margin. Similarly, a positive velocity and position feedback (PVPF) controller is proposed by Bhikkaji *et al.* in [73]. A sensorless active shunt control optimized using H_2 and H_∞ techniques is presented in [74] and achieves a 24 dB damping in the first resonant mode. In [75], a low-order feedforward controller is presented to compensate for the lateral oscillations of a PTS stemming from its mechanical resonances and, using this method, a system capable of imaging up to 125 μm-sized samples at a line scan rate of 122 Hz is obtained. This is about 15 times faster than a commercial system. A new vibration damping and tracking control technique based on integral force feedback (IFF) proposed in [76] increases the bandwidth of a positioner up to 255 Hz while the maximum achievable bandwidth with a commercial proportional-integral-derivative (PID) controller is only 26.1 Hz.

Integral resonant control (IRC) is another technique for suppressing the resonant mode of a PTS and is capable of scanning at a speed of $0.1 f_r$ [33]. Another approach which is widely used to mitigate this effect is to pre-shape the input signals so they do not excite the resonance of the stage [77]. Inversion-based controllers, such as inversion filters [78], which use inverted plant dynamics to suppress the resonant peaks have also been reported. However, inversion based controllers do not provide robustness to changes in system parameters which is critical in nanopositioning systems. The sliding mode control approach has also been investigated as a control design tool for robust tracking in nanopositioning systems [79], [80]. In [80], an intelligent integral backstepping sliding-mode control (IIBSMC) system using a recurrent neural network (RNN) is proposed for the three-dimensional motion control of a piezo-flexural nanopositioning stage (PFNS). This controller gives a better tracking of the reference contours over a PI controller and sliding mode control.

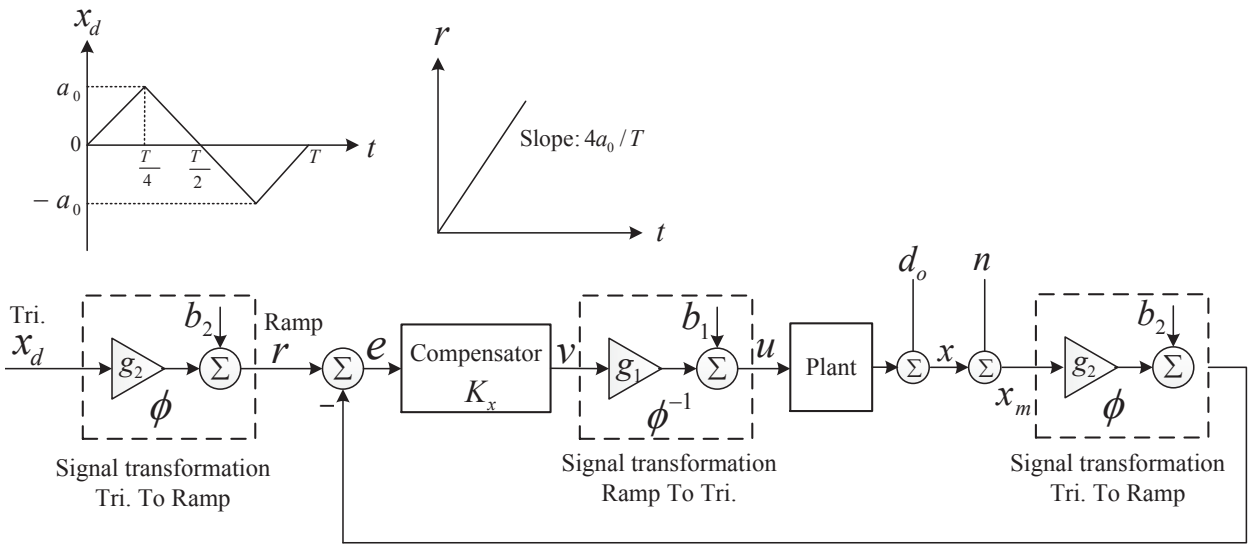

Fig. 14. Schematic diagram of the signal transformation method for triangular waveform tracking. Adapted from [68].

Other controllers, such as loop-shaping controllers and optimal controllers such as the linear quadratic Gaussian (LQG) controller and minimax LQG, have been implemented to improve tracking and scanning performances [81]–[84]. In [81], the internal reference model-based optimal LQG controller with a vibration compensator shown in Fig. 15 is proposed. It achieves approximately 14 dB damping in the resonant mode with a closed-loop bandwidth of about 850 Hz which results in a scanning speed up to 125 Hz. The modeling, identification, and design of a self-sensing method for compensating the vibration of a microelectromechanical system's (MEMS) nanopositioner is proposed in [85]. It utilizes a current sensor and charge sensor. Using the charge sensor output and a resonant controller, the resonant mode of a MEMS nanopositioner is attenuated by 18.45 dB which significantly compensates the vibration effect. A combined feedforward/feedback controller is proposed in [86], where the feedback controller maintains the robustness of the system against uncertainties and disturbances while the feedforward filter is designed via inversion of the nominal open-loop model to enhance the tracking performance. This controller achieves a bandwidth of 25% of the natural frequency of the first resonant peak and exhibits robustness against load variation on the stage.

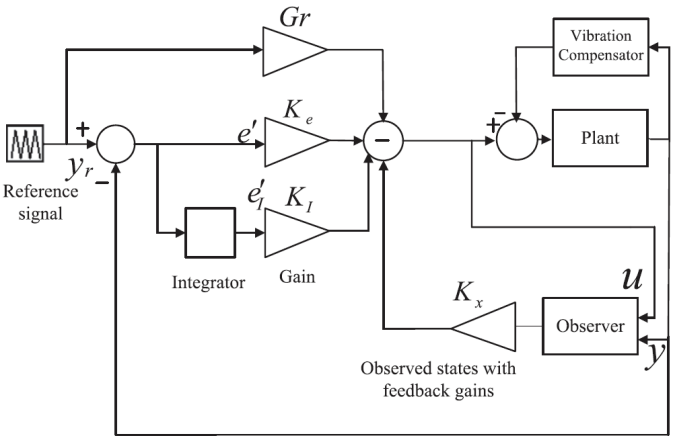

Fig. 15. Schematic diagram of an internal reference model-based optimal LQG controller for triangular waveform tracking. Adapted from [83].

2) Compensation of Hysteresis Effect: Two approaches are used to compensate for the hysteresis effects in piezoceramic actuator systems. One is the model-based feedforward approach and the other uses an improved feedback control technique. Various models have been proposed to describe the hysteresis behavior of piezoceramic actuators, such as the Preisach model [87], [88], the Prandtl-Ishlinskii model [89]–[91], the generalized Maxwell model [92], the Bouc-Wen model [79], [93], the Duhem model [94], and the polynomial model [95]. Of them, the Preisach model provides an accurate mathematical model for nonlinear hysteresis behavior and a more straightforward relationship between its input and output. It utilizes weighted hysteresis operators to predict the behavior of the hysteresis loop instead of differentiating the experimental data of the hysteresis loop. Therefore, this model is more suitable for control system design and real-time implementation than the other models. A detail about different hysteresis models are given in [96]

In [97], a complex Preisach hysteresis model is used to design a controller to control hysteresis but this controller produces distortions in scanned images at high frequencies because it does not take any steps to damp the resonant mode. In [98], a novel hysteresis operator and development of a rate-independent (RI) and rate-dependent (RD) hysteresis models for a PEA one-sided hysteresis which achieve significant compensation of the hysteresis effect are discussed. In [99], the least squares support vector machines (LSSVM) method in the domain of hysteresis modeling and compensation for a piezostage driven by a piezoelectric stack actuator (PSA) is presented. In addition, the LSSVM inverse model-based feedforward control combined with an incremental PID feedback

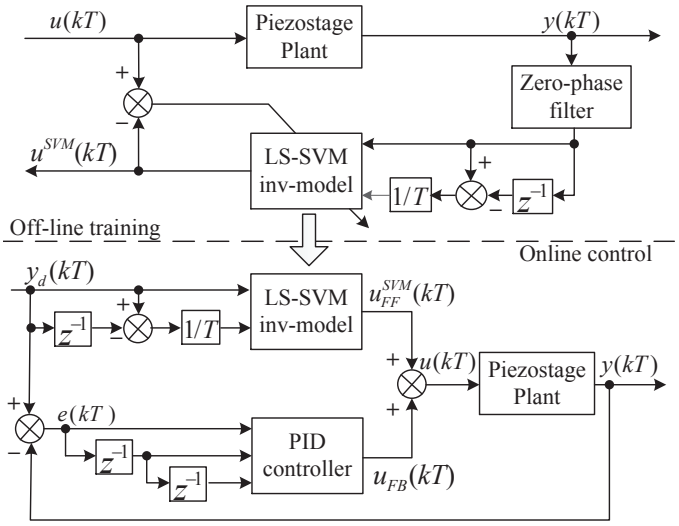

Fig. 16. LSSVM model based control for a piezostage system with a feedforward (FF) plus feedback (FB) hybrid controller. Adapted from [99].

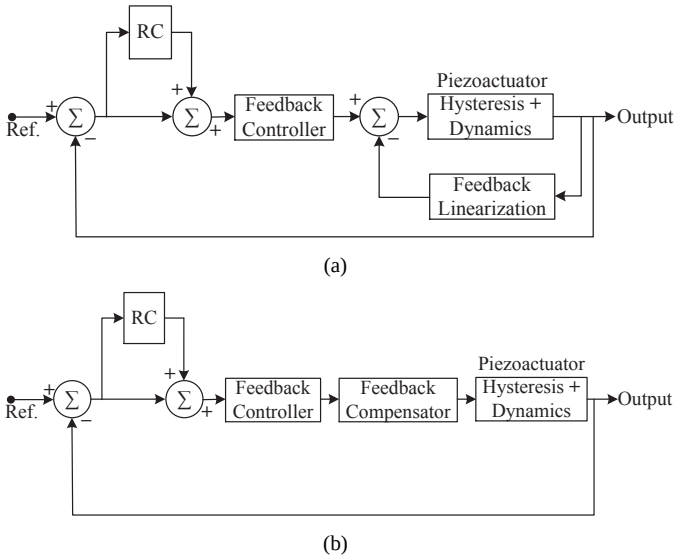

Fig. 17. Techniques to account for hysteresis in repetitive-control design: (a) feedback-linearization approach and (b) feedforward hysteresis compensation. Adapted from [114]

control designed to compensate the hysteresis nonlinearity is shown in Fig. 16. It achieves better results than the Bouc-Wen and modified Prandtl-Ishlinskii (MPI) model-based ones as well as both the stand-alone controllers.

Apart from model-based control methods, advanced controllers, such as the model predictive control (MPC) scheme [100], H_∞ [101], adaptive controller [102], [103], artificial neural networks (ANNs) [104], fuzzy logic control [105], repetitive control [106], sliding mode control [107], and iterative learning control (ILC) [97], have been designed to compensate the hysteresis effect in an AFM's PTS.

In 1981, a patent for reducing the hysteresis effect of PEA by using charge or current control rather than voltage was received [108]. Simply by regulating the current or charge, the hysteresis nonlinearity can be reduced from approximately 10% of the range to 1% [109]. Since then, although several studies have been conducted to combine charge control with other feedback control methods [110] to improve performance, charge control requires expensive hardware which increases the difficulty and cost of its implementation [111]. A sector-bounded H_∞ control approach to compensating for hysteresis effect is introduced in [101] and exhibits significant improvements in tracking, although its performance suffers in high frequency scanning, because it does not achieve much damping of the resonant modes. In [112] a robust adaptive controller is developed based on a reduced dynamic model under both unknown hysteresis nonlinearities and parameter uncertainties. Using this control framework the width of the hysteresis loops is reduced to a lower level of 1.05% with comparison to 17.25% obtained by the open-loop test under the same input frequencies.

In [97], the design of an ILC algorithm for achieving high-precision control of an AFM system based on the Preisach hysteresis model is presented. The greatest problem with iterative techniques is the time they take to iterate the compensator and their inability to control disturbances and cross-coupling. A frequency-based hysteresis compensation method for a PTS using ANNs presented in [104] and achieves good compensation of the hysteresis effect but at a low frequency of 1 Hz. This is in order to avoid vibration problems at high frequencies due to the excitation of the tube's resonance. In [113], a proposed feedforward strategy combined with a PI feedback controller for high-speed triangular trajectory tracking using a piezoelectric tube actuator (PTA) achieves significant compensation of the nonlinear hysteresis effect. Its better tracking performance also counteracts the effect of hysteresis, as examined in [114]. In [114], the hysteresis effect is accounted for in the control design, as shown in Fig. 17. A new control strategy named hysteresis creep inverse based robust adaptive model reference control (RAMRC) is proposed in [115] to reduce the effects of hysteresis, creep, and system drift in an SPM scanner to improve its positioning accuracy. The RAMRC approach uses a compensator to compensate for the hysteresis and creep and to tackle the unknown drift. The RAMRC also has a robust adaptive controller to explicitly deal with noise and disturbances.

3) Compensation of Creep Effect: A few methods for dealing with the creep effect have been proposed [53], [116]–[119]. The most commonly used approach in earlier AFMs was to allow sufficient time for the effect of creep to disappear. In [119], a Preisach type of creep compensator is used and its performance is evaluated in real-time applications; it achieves significant compensation of the creep effect. Creep, hysteresis, and vibration effects are minimized by implementing a proportional plus derivative high-gain feedback controller and feedforward controller in [120] and the control structure is shown in Fig. 18. An image reconstruction method for eliminating the creep effect in a Z–scanner in an AFM is proposed in [121]. In [118], a cascade model for the creep, hysteresis, and vibrational dynamics of piezo scanners is introduced, and the inverse dynamics are utilized to compensate for these effects in an open-loop fashion. In this work, each effect is

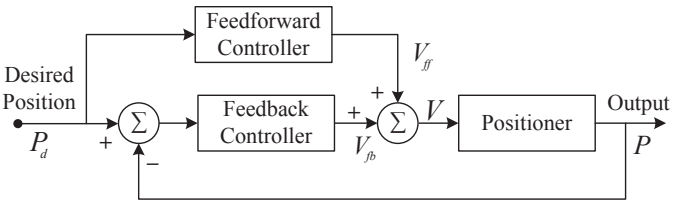

Fig. 18. Augmenting feedforward control with feedback. Adapted from [120].

identified separately using an optimal sensor for each of the x– and y–directions. Although the Preisach model produces better results for compensation of the creep effect, it fails to consider creep in a straightforward manner for piezoelectric materials and is computationally expensive. A better approach is to consider both creep and hysteresis in a single model using the Prandtl-Ishlinskii operator [122].

4) Compensation of Cross-coupling Effect: To compensate for the cross-coupling effect of a PTS in tapping-mode AFM imaging, an inversion-based iterative control (IIC) method is proposed in [44]. Although this technique works well for cross-coupling compensation, it only produces good-quality scanned images up to a 24.4 Hz scanning speed. A multi-input multi-output (MIMO) MPC controller with a damping compensator is proposed in [123] to compensate for the cross-coupling effect in the AFM's PTS. Using this method, the Y–to–X and X–to–Y cross-couplings are substantially reduced, by around 50 dB and 45 dB, respectively, at the resonances of the nanopositioner and enable the system to image up to a 125 Hz scanning speed. In [124], a MIMO IRC is implemented to speed up the performance of the AFM by considering the cross-coupling effects in the lateral and longitudinal axes of the PTS as symmetric. As shown in Fig. 19, a combination of a feedforward and IMC feedback control scheme is applied in a fabricated two degree-of-freedom (2–DoF) MEMS nanopositioner in [125] to ensure better tracking accuracy and settling time (and bandwidth) by compensating for the cross-coupling effect. The experimental results demonstrate the effectiveness of the proposed controllers which allow the 2–DOF system to have good tracking performance, with response times better than 110 ms, very high accuracy and rejection of cross-coupling and disturbances.

5) Compensate the Limitation of Probe: To increase the scanning speed of an AFM by reducing the cantilever's Q factor, an active impedance in the piezoelectric shunt control framework is proposed in [126]. By using this technique, scans are obtained on a 10 μm $\times$ 10 μm section of a calibration grating at a scanning speed of 60 μm/s. A modulated-demodulated control technique is applied in the amplitude modulation (AM) of an AFM to control the Q of its micro-cantilever [127]. This makes it possible to implement high-bandwidth PPF and resonant controllers using low-bandwidth reconfigurable controllers in the baseband and scan a 10 μm $\times$ 10 μm section of a calibration grating at a scanning speed of 78.2 μm/s. In [128], the cantilever's dynamics are optimized for high-speed operation by actively damping the Q factor of the cantilever which allows the amplitude of the oscillating

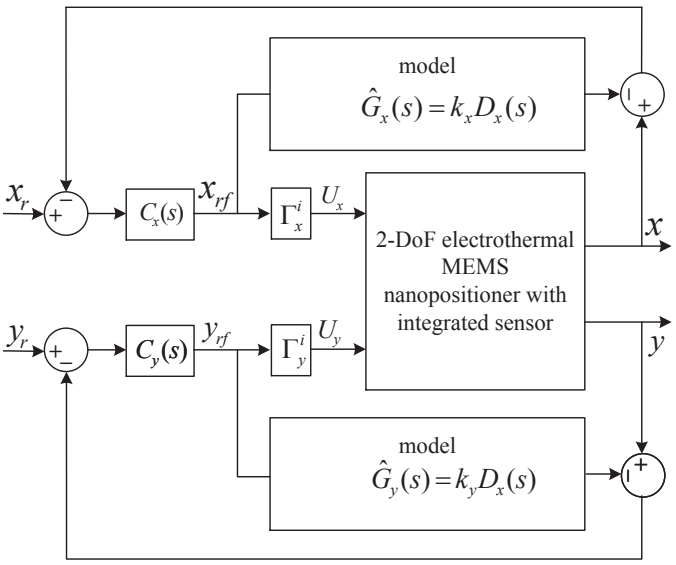

Fig. 19. Block diagram of the feedforward and IMC-feedback control of the 2–DOF electrothermal MEMS nanopositioner. Adapted from [125].

cantilever to respond more quickly to topographical changes. With this advancement, 80 μm $\times$ 80 μm high-speed tapping mode images are obtained at a scanning frequency of 15 Hz.

To improve AFM imaging requires precision positioning of its probe relative to the sample in 3D (x–y–z). However, that in the vertical z–axis direction this is still challenging because of issues such as the fact that the sample's topography is unknown. Generally, the probe-sample interaction, to which the probe-sample position is sensitive, is complicated. To overcome this problem, a novel current cycle feedback (CCF) iterative learning control (ILC) approach proposed in [129] achieves an eight times faster imaging speed for a contact mode AFM. A novel tip-sample estimation technique proposed in [130] to improve the bandwidth of the z-axis control loop results in an improved imaging bandwidth.

6) Compensate the Limitation of Measurement Unit: A Kalman observer can be used as a state-observer and noise filter [131]. The displacements of the PTSs are measured using the sub-nanometer resolution position sensors [132]. However, they add noise and disturbances to the displacement output which degrades an AFM's scanning performance. To remove this noise, a Kalman state observer is designed in [133] as a noise filter. To overcome the sensor noise a wide-bandwidth controller is implemented in [43] which provides reference tracking and damping of the actuator resonance, with an RMS displacement noise of about 0.34 nm. In this design, a piezoelectric strain sensor is combined with a capacitive sensor. The feedback loop utilizes a capacitive sensor at low frequencies and a piezoelectric sensor at high frequencies. This approach retains the low-frequency accuracy of the capacitive sensor and the wide bandwidth of the piezo sensor, while avoiding drift from the piezo sensor and wide band noise from the capacitive sensor. The closed-loop noise is reduced from 5 nm with the capacitive sensor to 0.34 nm with both sensors. By considering the limitations of the existing capacitive sensor

a piezoelectric force sensor is proposed in [32] along with a damping controller. This work has achieved an exceptionally high performance tracking controller without sacrificing stability margins.

7) Improvement of the Sampling Rate: To improve the sampling rate of the AFM system some research has been reported [134], [135]. A fast, high-resolution digital feedback controller for motion damping of low-k and high-Q cantilevers is constructed in [134]. The controller operates at a sampling rate of 625 kHz combined with fully resolved 16 bits 96 dB analog/digital dynamic range. In [135], integration of the feedback linearization and singular perturbation techniques is used to design a robust high-gain output feedback controller for an AFM that performs sample scanning at a high data sampling rate. This allows the cantilever tip to track the sample surface quickly and accurately.

B. New Scanning Patterns

To overcome the limitations of the conventional scanning method, three general approaches like spiral, cycloid, and Lissajous scanning methods have been proposed in the literature. A brief discuss about these scanning methods are given as follows.

1) Spiral Scanning Patterns: To overcome problems with a triangular reference signal, a non-raster scanning method, i.e., spiral scanning, is proposed in [136]. To generate a spiral pattern as shown in Fig. 20(b), the following signals are applied in the x– and y–axis, respectively, as shown in Fig. 20(a) [133]:

$$V_x(t) = r \sin \omega t; \tag{6}$$

$$V_y(t) = r \cos \omega t; \tag{7}$$

where r is the instantaneous radius at a time t which can be expressed as:

$$r = \frac{P}{2\pi} \omega t; \tag{8}$$

where the pitch, P is the distance between two consecutive intersections of the spiral curve with any line passing through its origin and is calculated as:

$$P = \frac{\text{spiral radius } \times \ 2}{\text{number of curves } - \ 1}; \tag{9}$$

where the $number\ of\ curves$ is defined as the number of times the spiral curve crosses the line $y = 0$. The total scanning time required for a complete spiral scan is

$$t_{\text{total}} = \frac{2\pi r_{\text{end}}}{P\omega}; \tag{10}$$

where r_{end} is the final value of the spiral radius, ω is the angular velocity, and P is the pitch, the distance between two consecutive intersections of the spiral curve with a line passing through its origin.

The image shown in Fig. 20(c) is obtained using the spiral scanning method at a 30 Hz scanning speed. A track-follow LQG controller is presented in [137] and applied for high-speed nanopositioning along Archimedean spiral trajectories, where it achieves very high-speed operation at scanning frequencies near the controller's bandwidth. A spiral technique with an H_∞ controller, which exploits the spiral-wise narrow-band frequency content of the reference signal to enable very high-speeds and accurate positioning, is proposed in [138]. The effectiveness of the spiral trajectory nanopositioning scheme over that of the conventional raster positioning pattern is examined in [139] by applying it to a MEMS-based scanning-probe data-storage setup for thermo-mechanical storage on a polymer medium. A spiral scanning method with an improved MPC scheme is applied to the PTS. By using this controller, the AFM is able to scan a 6 μm radius image within 2.04 s with a quality better than that obtained using the conventional raster pattern scanning method [133]. However, the initial scanning speed of the spiral scanning method is slow.

2) Cycloid Scanning Patterns: To overcome the problems in the spiral scanning method, a new sinusoidal scanning method, i.e., cycloid scanning, is introduced in [140] and shown in Fig. 21. To generate the cycloid pattern as shown in Fig. 21(b), the following signals are applied to the x– and y–axes, respectively, as shown in Fig. 21(a):

$$x(t) = \alpha t + r \sin \omega t; \tag{11}$$

$$y(t) = r \cos \omega t; \tag{12}$$

where $\omega = 2\pi f$ and f is the scan frequency, r is the amplitude of the input waveforms, and α is the ramp rate of the x input signal.

The image shown in Fig. 21(c) is obtained using the cycloid scanning method at a 30 Hz scanning speed. The significance of this method is that it does not require specialized apparatus to develop high-quality images at very high scanning speeds and works quite satisfactorily without the need to dampen the vibratory modes of the scanner which is a necessity in high-speed raster scanning AFMs [73]. However it has the problem that it scans the same area twice.

3) Lissajous Scanning Patterns: In [141] an alternative non-raster scanning method based on the Lissajous pattern, which allows much faster operation than ordinary scanning patterns, is introduced. Here, the two-dimensional Lissajous pattern is created by the interference of two single tone, constant amplitude, constant frequency waveforms in a two-dimensional space. Besides an extremely narrow frequency spectrum, the Lissajous scan trajectory possesses some unique properties that make it particularly well suited for high-speed imaging applications. An appealing capability of the Lissajous scan trajectory that cannot be achieved with a conventional scan trajectory, known as multi-resolution imaging. This pattern is achieved by applying the following signals to the X– and Y–piezos of the scanner, respectively:

$$x(t) = A_x \cos(\omega_x t); \tag{13}$$

$$y(t) = A_y \cos(\omega_y t); \tag{14}$$

where $\omega_x = 2\pi f_x$, $\omega_y = 2\pi f_y$, and A_x and A_y are positive constants representing the frequencies and amplitudes of the sinusoidal signals associated with the x– and y–axes,

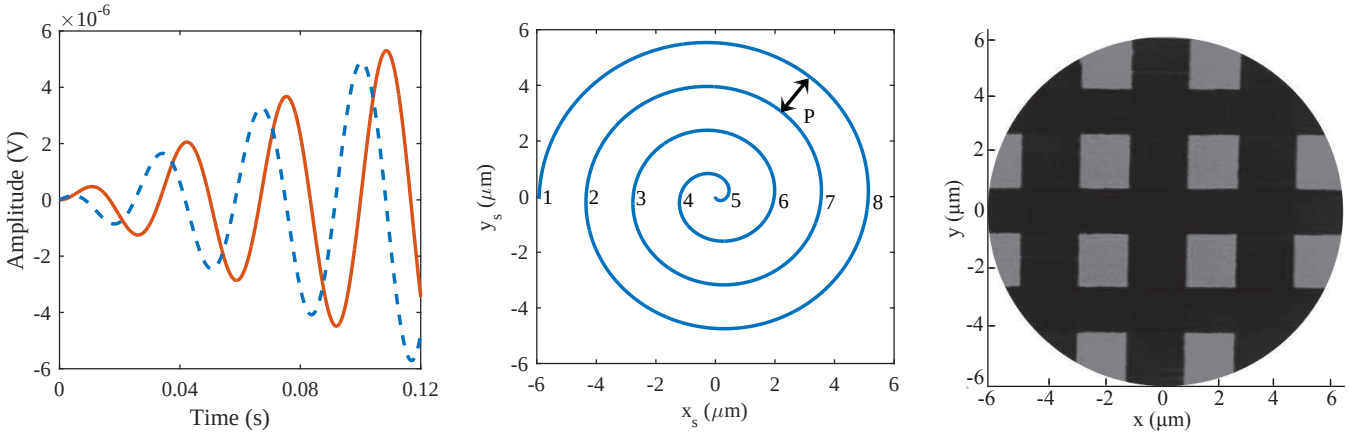

(a) (b) (c)

Fig. 20. (a) input signals applied to X–piezo (solid –) and Y–piezo (dotted - -) to generate spiral scan with ω = 188.50 rad/s; (b) spiral scan of 6 μm radius with $number\ of\ curves\ =$ 8; and (c) scanned AFM image using spiral scanning method.

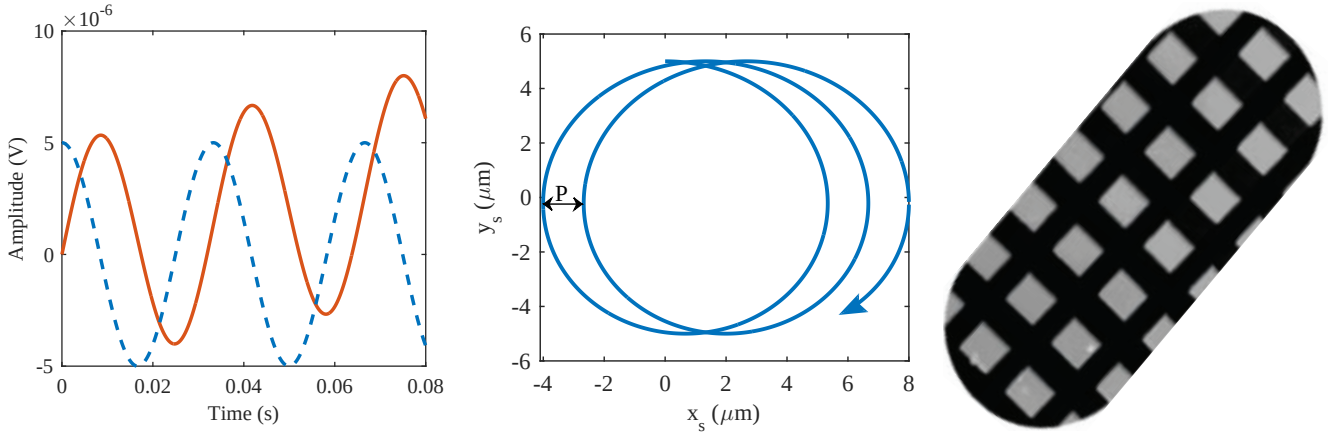

(a) (b) (c)

Fig. 21. (a) input signals applied to X–piezo (solid –) and Y–piezo (dotted - -) to generate cycloid scan with ω = 31.4 rad/s; (b) the cycloid trajectory of 5 μm radius; and (c) scanned AFM image using cycloid scanning method.

respectively. The full period of the Lissajous pattern is 1 s, which is calculated from the following relationship [141]:

$$T = \frac{1}{|f_x - f_y|}. \tag{15}$$

The generation of the Lissajous pattern is presented in Fig. 22. Figure 22(b) shows a Lissajous scanning pattern which is generated by applying input f_x = 8 Hz and f_y = 10 Hz with an amplitude A_x = A_y = 6 μm to the X–piezo and Y–piezo, respectively as shown in Fig. 22(a). Figure 22(c) presents a scanned AFM image obtained using the Lissajous scanning method.

C. Changing the Mechanical Structure

1) Changing the Mechanical Structure of the Scanner Stage: In addition to the control of the PTS, improved mechanical designs, such as stiff flexure-guided stages, also offer significant improvements in scanning speeds in an AFM, as discussed in [70], [142]–[144]. The capability of a flexure-based nanopositioner in an AFM to move the sample at a video rate is an important development for imaging biological samples as it has enabled researchers to record the dynamic behavior of biological processes. Recent nanopositioner designs have used MEMS technology [145]. MEMS devices possess the benefits of the miniaturization, batch production, and precision fabrication associated with the technology. The 2–DOF MEMS nanopositioner for an on-chip AFM reported in [146] is able to generate high-quality AFM images at scanning rates as fast as 100 Hz. At present scanners are limited in their scanning ranges. They are infeasible for scanning large samples in a reasonable time. However, to increase the feasible scanning area, a wide-area scanner that can scan over 46 $\times$ 46 μm^2 is developed in [147]. Improved mechanical design of the scanner can also limit the cross-coupling effect. In [148], the novel flexure-based piezoelectric stack-actuated XY nanopositioning stage presented significantly reduces the cross-coupling effect and, combined with IRC and feedforward control techniques, can achieve accurate high-speed scans up to 400 Hz.

Commercially available PTSs have very low resonance fre-

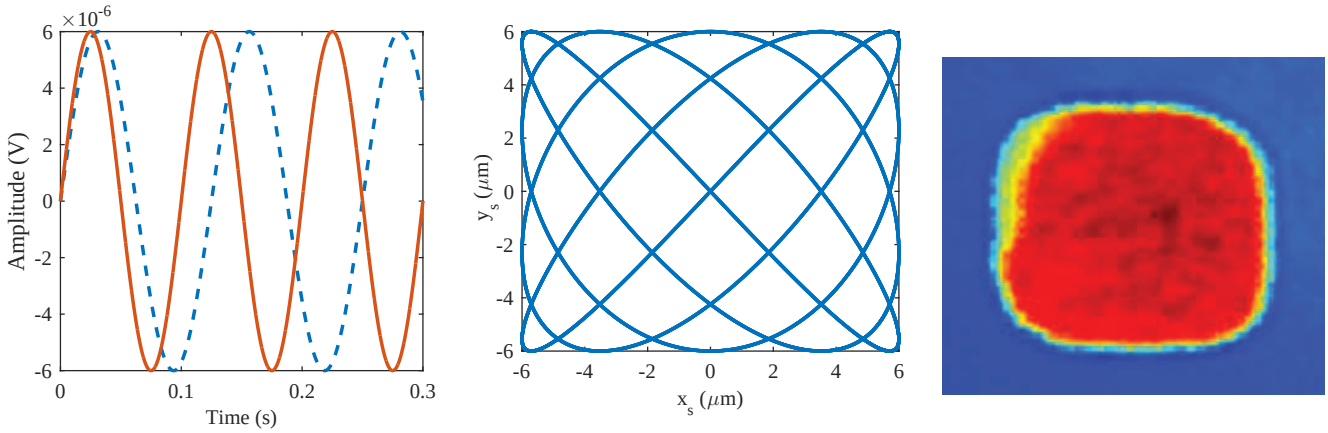

(a) (b) (c)

Fig. 22. (a) input signals applied to X–piezo (solid –) and Y–piezo (dotted - -) to generate Lissajous scan with f_x = 8 Hz and f_y = 10 Hz; (b) Lissajous scanning pattern; and (c) scanned AFM image using Lissajous scanning method.

quencies, e.g., a z50313cl PI scanner, a "scan by sample" type has resonance frequencies in both the X– and Y–directions of approximately 900 Hz and in the Z–direction of about 5 kHz. To overcome this problem, a novel monolithic serial-kinematic XYZ nanopositioner stage with a fixed-free configuration for high-speed AFM scanning is presented in [149] and shown in Fig. 23. It has resonance frequencies of 10 kHz, 7.5 kHz, and 64 kHz in the X–, Y–, and Z–directions, respectively. Using it, scanning performances with line rates up to 150 Hz are achieved. The high bandwidth nanopositioner proposed in [150] and shown in Fig. 24 successfully generates high-resolution images at a 200 Hz line rate with a 200 $\times$ 200 pixel resolution in closed-loop. Existing AFMs struggle due to limited bandwidth of the vertical feedback controller. To overcome this issue, the dual-stage vertical positioner proposed in [151] improves the feedback gain and increases its bandwidth from 83 Hz to 2.7 kHz. This improvement allows image quality to be retained with the speed increased 33 times or, alternatively, the feedback error can be reduced 33 times if the scanning speed is not increased. In [46], a XY flexure-based nanopositioning device with low cross-coupling between its two axes is proposed. In it, a H_∞ controller is introduced to minimize the effect of the resonant modes of the nanopositioner on the tracking of high-speed raster signals. In [152], the design of a two-axis, serial-kinematic high-speed scanner based on piezostack actuators is presented. The scanner's range is approximately 10 μm $\times$ 10 μm and the fast scanning axis is optimized for speed. The experimental results show a good correlation with simulation results, with a first resonance frequency of 29 kHz in the high-speed axis which is sufficient to achieve SPM line rates of approximately 4 kHz.

Also, a high-bandwidth, short-range vertical positioning stage integrated with a commercial SPM for dual-stage actuation is introduced in [153]. Dual-stage nanopositioners are becoming increasingly popular in applications such as AFM due to their unique ability to achieve long-range and high-speed operation but, due to the limitations of existing control schemes, struggle with some precision-positioning trajectories.

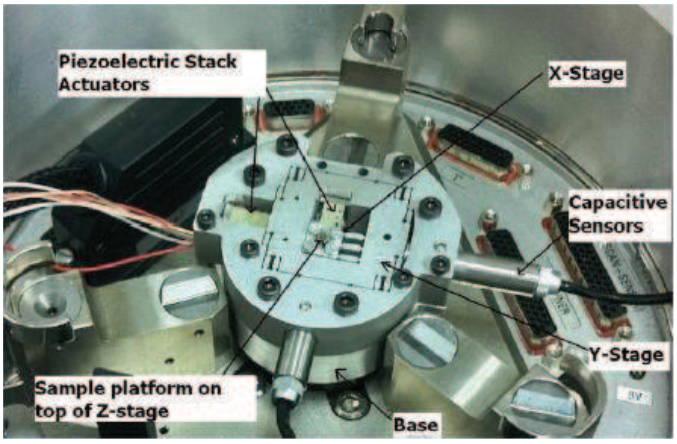

Fig. 23. High-speed serial-kinematic nanopositioner. Adapted from [149].

Specifically, short-range, low-speed inputs are typically diverted to the long-range actuator which, coincidentally, has a lower positioning resolution. To overcome this limitation, the novel dual-stage nanopositioner control framework shown in Fig. 25 is presented in [154] to achieve the positioning resolution required in applications in which the range and frequency are not inversely correlated. One more effective solution to overcome the limitations of the PTS is to design a scanner based on electromagnetic and electrostatic actuations rather than the conventional piezoelectric actuation principle. The advantage of electromagnetic actuation is that its dynamic behavior is linear. Also, it has a high open-loop bandwidth which enables its operation in both high-speed and high-resolution. Stemming from this fact, several positioners built upon electromagnetic actuation [155], [156] have been introduced. In [156] a novel dual-stage approach is presented which combined a low-speed, large-range scanner with a high-speed, short-range scanner as shown in Fig. 26. In this design, the short-range scanner is designed using an electromagnetic actuation principle whereas for the large-range scanner, conventional piezo actuation is used. An AFM based

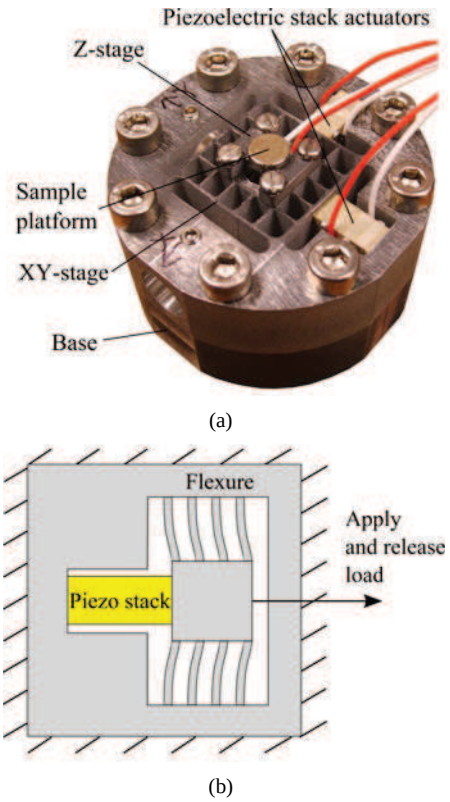

Fig. 24. (a) Improved XYZ nanopositioner and (b) preload method. Adapted from [150]

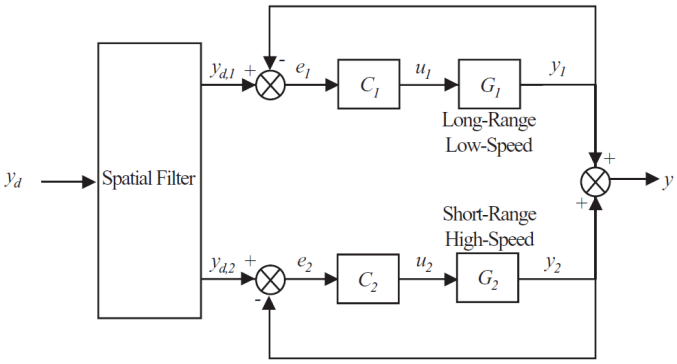

Fig. 25. Range-based control scheme. Adapted from [154].

on this dual stage design can scan an area of 2 μm $\times$ 2 μm with a resolution of 655 $\times$ 200 pixels at a scan rate of 1.25 frames/s. In order to increase the measurement range of an AFM scanning system, a combination of a PEA and an electromagnetic actuator is presented in [157]. In this design while the piezoelectric actuation positioner (PAP) provides high-speed scanning with nanometer resolution in the z–axis, the precision electromagnetic positioner (PEP) is capable of 1 mm^2 large field positioning with 20 nm RMS error in the xy–axes. The overall design of the stage consists of 4 pairs of electromagnetic actuators, monolithic serial flexure guidance with compression springs, an eddy current damper, and a commercial z-axis PAP.

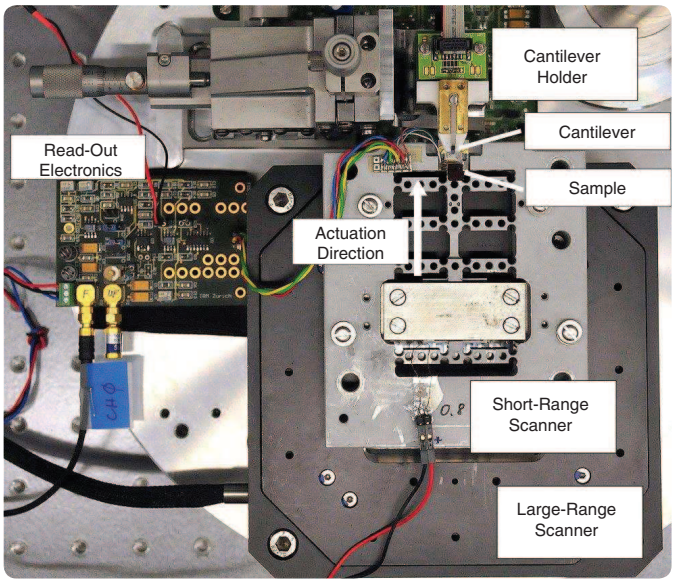

Fig. 26. Photograph of a dual-stage scanner system, showing the single-axis short-range scanner mounted on the three-axis large-range positioning stage. Adapted from [156].

D. Changing the Mechanical Structure of the Probe

Apart from the limitations of scanners, the size of the probe especially cantilever has an important effect in AFM imaging. As reducing the cantilever's dimensions reduces its mass and increases its resonance frequency while maintaining the spring constant at reasonable values, small cantilevers enable imaging at high-speed [158]. By considering this fact Ando *et al.* developed small cantilevers with high resonance frequencies (450-650 kHz) and small spring constants (150-280 pN/nm) to meet the high-speed AFM imaging [159]. In [59], an AFM head integrated with a small cantilever which can take tapping-mode images approximately 510-times faster than the same AFM system using a large cantilever is proposed. In [160] a robust feedback controller for a highly coupled, strongly nonlinear (hysteresis and creep) and vibrating 2-DOF piezo-cantilever is presented.

XI. Future Challenges and Conclusion

As the extensive applications of AFMs in nanotechnology have become more demanding, AFM control is currently a fundamental part of research in this field. To achieve the fast operation of an AFM according to the demands of modern science, it is necessary to address the issues which limit its imaging performance. This paper presents a survey of recent methodologies and technologies aimed at maximizing its performance. From the literature, it is clear that, to improve the scanning speed and image quality of an AFM, some researchers have concentrated on its scanning unit and developed improved control techniques such as feedback, feedforward, iteration and sensorless methods, or changed the mechanical structure of the scanner stage and probe, some have enhanced the bandwidth of the cantilever, some have used different scanning techniques, and others have used different control techniques to compensate the limitations of the measurement

units. Based on this, it is evident that a significant volume of research on high-speed AFM imaging has been reported over the past two decades which may falsely lead one to conclude that 'what could have been done has already been done'. However, as the preceding discussion indicates, significant improvements can be achieved in future by addressing the following issues.

A. System modeling

From the literature review, it is clear that the inclusion of the unmodeled dynamics for the 3D positioning of an AFM system has not yet been satisfactorily considered in the control design. Proper mathematical modeling is one of the key factors for obtaining the desired control responses from any physical system. To meet the present demand for high-speed AFM imaging, researchers should concentrate on the modeling of the vertical dynamics of the AFM. This is a critical part for the system modeling. Besides considering the effects of different nonlinearities and the cross-coupling issue, future research should consider the dynamics of the cantilever beam and the dynamics of the interaction between the sample and the cantilever tip. In most AFM systems, position is measured using a capacitive position sensor which has added noise and it creates a time delay in the system response that results in significant detrimental effects on the control system performance. To overcome this limitation, the sensor dynamics should be considered in the uncertain system modeling. Apart from these limitations, the hysteresis effect in the scanner still remains a challenging issue in terms of its rate-dependent modeling and inverse construction.

B. Control design

Most of the high-speed imaging research for AFMs focuses on only lateral axis control while leaving the vertical axis to be controlled using the in-built PI controller which has a low bandwidth due to the resonant modes of the PTS. Also, in existing AFM control designs, robustness issues are often overlooked. On the other hand, existing control approaches are somewhat limited by the complexity of their implementation which, in some cases, requires modifications to the hardware. For these reasons, the use of advanced control for an AFM still requires significant research to meet the requirements of fast scanning, especially in applications in the field of medical science. To improve the overall performance of an AFM, one possible solution could be to consider a parallel structure in a robust control framework consisting of two controllers with two different objectives together with an uncertainty model of the system. One controller could aim to track the reference trajectories at a high-speed with high accuracy as well as deal with system uncertainties and the other could suppress structural vibration. To obtain a more robust performance, this feedback controller could be used with a sinusoidal scanning method and be capable of scanning a $100\ \mu\text{m} \times 100\ \mu\text{m}$ area near the PTS's resonance frequency for biological samples. This technique would minimize both the complexity and cost of the control system.

C. Mechanical Design

Currently, different types of flexure-guided nanopositioners, such as MEMS nanopositioners, have been used as alternatives to the PTS. However, the design of such a scanner is complex and very expensive. On the other hand, as a PTS is easily manufactured, widely available and inexpensive, its widespread use is likely to continue well into the future. Therefore, reducing its complexity and cost should be taken into account in the future design of the mechanical structure. The cantilever is one of the bottlenecks in high-speed imaging using an AFM in the tapping mode due its low acquisition rates. New cantilever designs and controllers could be a future research topic.

D. Scanning Method

Over the past two decades, research aimed at overcoming the limitations of existing scanning methods has resulted in spiral, cycloid, and Lissajous scanning methods. However, the spiral scanning method suffers due to the slow initial scanning speed while the cycloid scans the same area twice. On the other hand, as the analysis and design of Lissajous scan trajectories are challenging owing to the nonlinear relationship between the harmonic actuation frequencies and resulting durations and shapes of the scan trajectories. Hence, there is a great deal of scope for further research in this area.

E. Measurement Unit

In the past two decades, some research has been conducted with the aim of improving the performance of an AFM's measurement units. One of the foremost challenges of position sensing is to achieve high resolution and accuracy over a large bandwidth range. Although one possible solution is the collaborative use of multiple sensors, this will increase the overall cost. Also, the existing PSPD struggles with some issues as it has some glasses which increase the overall weight of the AFM's head and its sensitivity is limited.

REFERENCES

[1] G. Binnig and D. P. E. Smith, "Single tube three-dimensional scanner for scanning tunneling microscopy," *Rev. Sci. Instrum.*, vol. 57, no. 8, pp. 1688–1689, Aug. 1986.

[2] G. Binnig and H. Rohrer, "Scanning tunneling microscopy from birth to adolescence," *Reviews of Modern Physics*, vol. 59, no. 3, pp. 615–625, Jul. 1987.

[3] M. S. Rana, "High Performance Control of an Atomic Force Microscope for Faster Image Scanning," Ph.D. dissertation, University of New South Wales, Australia, 2014.

[4] U. Drig, D. W. Pohl, and F. Rohner, "Near-field optical-scanning microscopy," *Journal of Physics*, vol. 59, no. 10, pp. 3318–3327, May 1986.

[5] A. Majumdar, "Scanning thermal microscopy," *Annu. Rev. Mater. Sci.*, vol. 29, pp. 505–585, 1999.

[6] G. K. Binnig, C. F. Quate, and C. Gerber, "Atomic force microscope," *Physical Review Letters*, vol. 56, no. 9, pp. 930–933, Mar. 1986.

[7] U. Hartmann, "Magnetic force microscopy," *Annu. Rev. Mater. Sci.*, vol. 29, pp. 53–87, 1999.

[8] C. C. Williams and H. K. Wickramasinghe, "Microscopy of chemical-potential variations on an atomic scale," *Nature*, vol. 344, pp. 317–319, 1990.

[9] P. Girard, "Electrostatic force microscopy: principles and some applications to semiconductors," *Nanotechnology*, vol. 12, no. 4, pp. 485–490, Oct. 2001.

[10] P. Hansma, B. Drake, O. Marti, S. Gould, and C. Prater, "The scanning ion-conductance microscope," *Science*, vol. 243, no. 4891, pp. 641–643, 1989.

[11] J. Matey and J. Blanc, "Scanning capacitance microscopy," *Annu. Rev. Mater. Sci.*, vol. 57, pp. 1437–1444, 1999.

[12] M. S. Rana, H. R. Pota, and I. R. Petersen, "Performance of sinusoidal scanning with MPC in AFM imaging," *IEEE/ASME Trans. Mechatronics*, vol. 20, no. 1, pp. 73–83, Feb. 2015.

[13] C. Gerber and H. P. Lang, "How the doors to the nanoworld were opened," *Nature Nanotechnology*, vol. 1, pp. 3–5, Oct. 2006.

[14] M. Berger, "A key tool for nanotechnology: Atomic force microscopy," *http://www.nanowerk.com/spotlight/spotid=4876.php*, Mar. 2008.

[15] M. Salerno, "Microscopia 2000," *http://digilander.libero.it/citizenz/*, 1999.

[16] Park Systems, "Park atomic force microscope," *http://www.parkafm.com/*.

[17] J. Hou, L. Liu, Z. Wang, Z. Wang, N. Xi, Y. Wang, C. Wu, Z. Dong, and S. Yuan, "AFM-based robotic nano-hand for stable manipulation at nanoscale," *IEEE Trans. Autom. Sci. Eng.*, vol. 10, no. 2, pp. 285–295, April 2013.

[18] T. Ando, T. Uchihashi, and N. Kodera, "High-speed AFM and applications to biomolecular systems," *Annual review of biophysics*, vol. 42, pp. 393–414, 2013.

[19] M. S. Rana, H. R. Pota, and I. R. Petersen, "The design of model predictive control for an AFM and its impact on piezo nonlinearities," *European Journal of Control*, vol. 20, no. 4, pp. 188–198, Apr. 2014.

[20] T. Ando, "High-speed AFM imaging," *Curr. Opin. Struct. Biol.*, vol. 28, pp. 63–68, Oct. 2014.

[21] M. S. Rana, H. Pota, and I. R. Petersen, "Error compensation in atomic force microscope scanned images," *Micro & Nano Letters, IET*, pp. 1–3, Oct. 2015.

[22] B. Bhushan, *Springer Handbook of Nanotechnology*. New York, NY, USA: Springer, 2006.

[23] M. Fairbairn and S. O. R. Moheimani, "Resonant control of an atomic force microscope micro-cantilever for active Q control," *Rev. Sci. Instrum.*, vol. 83, pp. 083 708 (1–9), Aug. 2012.

[24] A. A. Eielsen, J. Gravdahl, and K. Pettersen, "Adaptive feed-forward hysteresis compensation for piezoelectric actuators," *Rev. Sci. Instrum.*, vol. 83, no. 8, pp. 085 001–085 001–8, Aug 2012.

[25] D. Mehlfeldt, H. Weckenmann, and G. Sthr, "Modeling of piezoelectrically actuated fuel injectors," *Mechatronics*, vol. 18, no. 56, pp. 264–272, Jun. 2008.

[26] S. Z. S. Hassen, M. Heurs, E. H. Huntington, I. R. Petersen, and M. R. James, "Frequency locking of an optical cavity using linearquadratic gaussian integral control," *Journal of Physics B: Atomic, Molecular and Optical Physics*, vol. 42, no. 17, pp. 175 501–175 501–10, 2009.

[27] Y. Takeuchi, Y. Sakaida, K. Sawada, and T. Sata, "Development of a 5-axis control ultraprecision milling machine formicromachining based on non-friction servomechanisms," *CIRP Annals - Manufacturing Technology*, vol. 49, no. 1, pp. 295 – 298, 2000.

[28] M. Robiony, F. Polini, F. Costa, N. Zerman, and P. M., "Ultrasonic bone cutting for surgically assisted rapid maxillary expansion (SARME) under local anaesthesia," *Int. J. Oral Maxillofac. Surg.*, vol. 36, no. 3, pp. 267–269, 2007.

[29] S. M. Salapaka and M. V. Salapaka, "Scanning probe microscopy," *IEEE Control Systems*, vol. 28, no. 2, pp. 65–83, Apr. 2008.

[30] L. D. Mauck and C. S. Lynch, "Piezoelectric hydraulic pump development," *J. Intell. Mater. Syst. Struct.*, vol. 11, no. 10, pp. 758–764, Oct. 2000.

[31] Y. Zhang, G. Liu, and J. Hesselbach, "On development of a rotary-linear actuator using piezoelectric translators," *IEEE/ASME Trans. Mechatronics*, vol. 11, no. 5, pp. 647–650, Oct. 2006.

[32] A. J. Fleming, "Nanopositioning system with force feedback for high-performance tracking and vibration control," *IEEE/ASME Trans. Mechatronics*, vol. 15, no. 3, pp. 433–447, Jun. 2010.

[33] B. Bhikkaji and S. O. R. Moheimani, "Integral resonant control of a piezoelectric tube actuator for fast nanoscale positioning," *IEEE/ASME Transactions on Mechatronics*, vol. 13, no. 5, pp. 530–537, October 2008.

[34] M. S. Rana, H. Pota, and I. R. Petersen, "Approach for improved positioning of an atomic force microscope piezoelectric tube scanner," *Micro & Nano Letters, IET*, vol. 9, no. 6, pp. 407–411, Jun. 2014.

[35] S. Kuiper and G. Schitter, "Active damping of a piezoelectric tube scanner using self-sensing piezo actuation," *Mechatronics*, vol. 20, no. 6, pp. 656–665, Sep. 2010.

[36] H. R. Pota, S. O. R. Moheimani, and M. Smith, "Resonant controller for smart structures," *Smart Materials and Structures*, vol. 11, no. 1, pp. 1–8, February 2002.

[37] M. S. Rana, H. R. Pota, I. R. Petersen, and Habibullah, "High performance control of a PZT scanner for fast nanoscale positioning of atomic force microscope," in *Proceedings of the Australian Control Conference (AUCC)*, Sydney, Nov. 2012, pp. 464–469.

[38] G.-Y. Gu, L.-M. Zhu, and C.-Y. Su, "Integral resonant damping for high-bandwidth control of piezoceramic stack actuators with asymmetric hysteresis nonlinearity," *Mechatronics*, vol. 24, no. 4, pp. 367–375, 2014, vibration control systems.

[39] C. Canale, B. Torre, D. Ricci, and P. Braga, "Recognizing and avoiding artifacts in atomic force microscopy imaging," in *Atomic Force Microscopy in Biomedical Research*, ser. Methods in Molecular Biology, P. C. Braga and D. Ricci, Eds. Humana Press, 2011, vol. 736, pp. 31–43.

[40] M. S. Rana, H. R. Pota, I. R. Petersen, and H. Habibullah, "Effect of improved tracking for atomic force microscope on piezo nonlinear behavior," *Asian Journal of Control*, vol. 17, no. 3, pp. 747–761, May 2015.

[41] M. S. Rana, H. R. Pota, and I. R. Petersen, "Creep, hysteresis, and vibration effects attenuation in an AFM PTS," in *European Control Conference (ECC)*, Jun. 2014, pp. 2022–2027.

[42] G.-Y. Gu and L.-M. Zhu, "Comparative experiments regarding approaches to feedforward hysteresis compensation for piezoceramic actuators," *Smart Materials and Structures*, vol. 23, no. 9, pp. 095 029–095 029–40, 2014.

[43] A. J. Fleming, A. Wills, and S. Moheimani, "Sensor fusion for improved control of piezoelectric tube scanners," *IEEE Trans. Control Syst. Technol.*, vol. 16, no. 6, pp. 1265–1276, Nov. 2008.

[44] Y. Wu, J. Shi, C. Su, and Q. Zou, "A control approach to cross-coupling compensation of piezotube scanners in tapping-mode atomic force microscope imaging," *Rev. Sci. Instrum.*, vol. 80, no. 4, pp. 043 709–043 709–10, Apr. 2009.

[45] M. S. Rana, H. R. Pota, and I. R. Petersen, "Cross-coupling effect compensation of an AFM piezoelectric tube scanner for improved nanopositioning," in *Proc. IEEE Amer. Control Conf.*, Jun. 2014, pp. 2456–2461.

[46] Y. K. Yong, K. Liu, and S. O. R. Moheimani, "Reducing cross-coupling in a compliant XY nanopositioner for fast and accurate raster scanning," *IEEE Transactions on Control Systems Technology*, vol. 18, no. 5, pp. 1172–1179, Sep. 2010.

[47] M. S. Rana, H. R. Pota, and I. R. Petersen, "High-speed AFM image scanning using observer-based MPC-Notch control," *IEEE Trans. Nanotechnol.*, vol. 12, no. 2, pp. 246–254, Mar. 2013.

[48] B. Bhikkaji and S. O. R. Moheimani, "Fast scanning using piezoelectric tube nanopositioners: A negative imaginary approach," in *Proceedings of the IEEE/ASME International Conference on Advanced Intelligent Mechatronics (AIM)*, Singapore, July 2009, pp. 274–279.

[49] D. Ricci and P. C. Braga, "Recognizing and avoiding artifacts in atomic force microscopy imaging," *Atomic Force Microscopy: Biomedical Methods and Applications*, vol. 242, pp. 25–37, 2004.

[50] A. Visintin, *Differential Models of Hysteresis*. Berlin,Germany: Springer-Verlag, 1994.

[51] N. Chuang and I. R. Petersen, "Robust H^∞ control in nanopositioning," *Control Theory Applications, IET*, vol. 6, no. 13, pp. 1993–2001, Sep. 2012.

[52] H. Adriaens, W. De Koning, and R. Banning, "Modeling piezoelectric actuators," *IEEE/ASME Trans. Mechatronics*, vol. 5, no. 4, pp. 331–341, Dec. 2000.

[53] H. Jung, J. Y. Shim, and D. Gweon, "New open-loop actuating method of piezoelectric actuators for removing hysteresis and creep," *Rev. Sci. Instrum.*, vol. 71, no. 9, pp. 3436–3440, September 2000.

[54] W. D. Callister and D. G. Rethwisch, *Materials Science and Engineering: An Introduction*, 7th ed. New York: John Wiley and Sons, Inc., 2007.

[55] S. O. R. Moheimani, "Invited review article: Accurate and fast nanopositioning with piezoelectric tube scanners: Emerging trends and future challenges," *Rev. Sci. Instrum.*, vol. 79, no. 7, pp. 071 101(1–11), July 2008.

[56] R. Proksch, "Multifrequency, repulsive-mode amplitude-modulated atomic force microscopy," *Applied Physics Letters*, vol. 89, no. 11, pp. 113 121–113 121–3, 2006.

[57] L. Lin, "Atomic Force Microscopy Recognition Imaging for Epigenetic Mapping," Ph.D. dissertation, Arizona State University, USA, 2009.

[58] B. Rogers, T. Sulchek, K. Murray, D. York, M. Jones, L. Manning, S. Malekos, B. Beneschott, J. Adams, H. Cavazos, and S. Minne,

"High speed tapping mode atomic force microscopy in liquid using an insulated piezoelectric cantilever," *Rev. Sci. Instrum.*, vol. 74, no. 11, pp. 4683–4686, Nov. 2003.

[59] J. D. Adams, A. Nievergelt, B. W. Erickson, C. Yang, M. Dukic, and G. E. Fantner, "High-speed imaging upgrade for a standard sample scanning atomic force microscope using small cantilevers," *Rev. Sci. Instrum.*, vol. 85, no. 9, pp. 093 702–093 702–7, Sep. 2014.

[60] M. S. Rana, H. R. Pota, I. R. Petersen, and Habibullah, "Improvement of the tracking accuracy of an AFM using MPC," in *8th IEEE Conference on Industrial Electronics and Applications (ICIEA)*, Jun. 2013, pp. 1681–1686.

[61] I. A. Mahmood and S. O. R. Moheimani, "Making a commercial atomic force microscope more accurate and faster using positive position feedback control," *Rev. Sci. Instrum.*, vol. 80, no. 6, pp. 063 705–063 705–8, Jun. 2009.

[62] A. J. Fleming, "A review of nanometer resolution position sensors: Operation and performance," *Sensors and Actuators A: Physical*, vol. 190, pp. 106–126, 2013.

[63] M. J. Higgins, R. Proksch, J. E. Sader, M. Polcik, S. Mc Endoo, J. P. Cleveland, and S. P. Jarvis, "Noninvasive determination of optical lever sensitivity in atomic force microscopy," *Rev. Sci. Instrum.*, vol. 77, no. 1, pp. –, 2006.

[64] G. Schitter, G. Fantner, P. Thurner, and P. Hansma, "On recent developments for high-speed atomic force microscopy," in *IEEE/ASME International Conference on Advanced Intelligent Mechatronics*, 2005, pp. 261–264.

[65] D. Abramovitch, S. Andersson, L. Y. Pao, and G. Schitter, "A tutorial on the mechanisms, dynamics, and control of atomic force microscopes," in *American Control Conference, 2007*, Jul. 2007, pp. 3488–3502.

[66] M. E. Taylor, "Dynamics of piezoelectric tube scanners for scanning probe microscopy," *Rev. Sci. Instrum.*, vol. 64, no. 1, pp. 154–158, Jan. 1993.

[67] S. Devasia, E. Eleftheriou, and S. O. R. Moheimani, "A survey of control issues in nanopositioning," *IEEE Transactions on Control Systems Technology*, vol. 15, no. 5, pp. 802–823, Sep. 2007.

[68] A. Bazaei, Y. K. Yong, S. O. R. Moheimani, and A. Sebastian, "Tracking of triangular references using signal transformation for control of a novel AFM scanner stage," *IEEE Transactions on Control Systems Technology*, vol. 20, no. 2, pp. 453–464, Mar. 2012.

[69] H. R. Pota, S. O. R. Moheimani, and M. Smith, "Resonant controllers for flexible structures," in *Proceedings of the 38th IEEE Conference on Decision and Control (CDC)*, vol. 1, Phoenix, Arizona, USA, Dec. 1999, pp. 631–636.

[70] G. Schitter, K. J. Astrom, B. E. DeMartini, P. J. Thurner, K. L. Turner, and P. K. Hansma, "Design and modeling of a high-speed AFM-scanner," *IEEE Trans. Control Syst. Technol.*, vol. 15, no. 5, pp. 906–915, Sep. 2007.

[71] T. Tuma, A. Sebastian, W. Haberle, J. Lygeros, and A. Pantazi, "Impulsive control for fast nanopositioning," *Nanotechnology*, vol. 22, no. 13, pp. 135 501–1135 501–6, Feb. 2011.

[72] A. Bazaei, S. O. R. Moheimani, and Y. K. Yong, "Improvement of transient response in signal transformation approach by proper compensator initialization," *IEEE Trans. Control Syst. Technol.*, vol. 22, no. 2, pp. 729–736, Mar. 2014.

[73] B. Bhikkaji, M. Ratnam, A. J. Fleming, and S. O. R. Moheimani, "High-performance control of piezoelectric tube scanners," *IEEE Transactions on Control Systems Technology*, vol. 15, no. 5, pp. 853–866, Sep. 2007.

[74] S. S. Aphale, A. J. Fleming, and S. O. R. Moheimani, "High speed nano-scale positioning using a piezoelectric tube actuator with active shunt control," *Micro & Nano Letters, IET*, vol. 2, no. 1, pp. 9–12, Mar. 2007.

[75] G. Schitter and A. Stemmer, "Identification and open-loop tracking control of a piezoelectric tube scanner for high-speed scanning-probe microscopy," *IEEE Trans. Control Syst. Technol.*, vol. 12, no. 3, pp. 449–454, May 2004.

[76] Y. R. Teo, D. Russell, S. S. Aphale, and A. J. Fleming, "Optimal integral force feedback and structured PI tracking control: Application for high speed confocal microscopy," *Mechatronics*, vol. 24, no. 6, pp. 701–711, Sep. 2014.

[77] Y. Li and J. Bechhoefer, "Feedforward control of a closed-loop piezoelectric translation stage for atomic force microscope," *Rev. Sci. Instrum.*, vol. 78, no. 1, pp. 013 702–013 702–8, Jan. 2007.

[78] D. Y. Abramovitch, S. Hoen, and R. Workman, "Semi-automatic tuning of PID gains for atomic force microscopes," in *Proceedings of the American Control Conference (ACC)*, Seattle, Washington, USA, Jun. 2008, pp. 2684–2689.

[79] Y. Li and Q. Xu, "Adaptive sliding mode control with perturbation estimation and PID sliding surface for motion tracking of a piezo-driven micromanipulator," *IEEE Trans. Control Syst. Technol.*, vol. 18, no. 4, pp. 798–810, July 2010.

[80] F.-J. Lin, S.-Y. Lee, and P.-H. Chou, "Intelligent integral backstepping sliding-mode control using recurrent neural network for piezo-flexural nanopositioning stage," *Asian Journal of Control*, vol. 17, no. 6, pp. 1–17, Nov. 2015.

[81] Habibullah, H. R. Pota, I. R. Petersen, and M. S. Rana, "Creep, hysteresis, and cross-coupling reduction in the high-precision positioning of the piezoelectric scanner stage of an atomic force microscope," *IEEE Trans. Nanotechnol.*, vol. 12, no. 6, pp. 1125–1134, Nov. 2013.

[82] C. Lee and S. M. Salapaka, "Robust broadband nanopositioning: fundamental trade-offs, analysis, and design in a two-degree-of-freedom control framework," *Nanotechnology*, vol. 20, pp. 035 501–035 516, Dec. 2009.

[83] H. Habibullah, H. R. Pota, I. R. Petersen, and M. S. Rana, "Tracking of triangular reference signals using LQG controllers for lateral positioning of an AFM scanner stage," *IEEE/ASME Trans. Mechatronics*, vol. 19, no. 4, pp. 1105–1114, Aug. 2014.

[84] J. Dong, S. M. Salapaka, and P. M. Ferreira, "Robust control of a parallel- kinematic nanopositioner," *ASME Journal of Dynamic Systems, Measurement, and Control*, vol. 130, no. 4, pp. 041 007(1–15), Jun. 2008.

[85] S. I. Moore and S. O. R. Moheimani, "Vibration control with MEMS electrostatic drives: A self-sensing approach," *IEEE Trans. Control Syst. Technol.*, pp. 1–8, 2014.

[86] M. Kara-Mohamed, W. Heath, and A. Lanzon, "Enhanced tracking for nanopositioning systems using feedforward/feedback multivariable control design," *Control Systems Technology, IEEE Transactions on*, vol. 23, no. 3, pp. 1003–1013, May 2015.

[87] G. Song, J. Zhao, X. Zhou, and J. A. De Abreu-Garcia, "Tracking control of a piezoceramic actuator with hysteresis compensation using inverse preisach model," *IEEE/ASME Trans. Mechatronics*, vol. 10, no. 2, pp. 198–209, Apr. 2005.

[88] A.-F. Boukari, J.-C. Carmona, G. Moraru, F. Malburet, A. Chaaba, and M. Douimi, "Piezoactuators modeling for smart applications," *Mechatronics*, vol. 21, no. 1, pp. 339–349, 2011.

[89] G.-Y. Gu, L.-M. Zhu, and C.-Y. Su, "Modeling and compensation of asymmetric hysteresis nonlinearity for piezoceramic actuators with a modified prandtl-ishlinskii model," *IEEE Transactions on Industrial Electronics*, vol. 61, no. 3, pp. 1583–1595, March 2014.

[90] M. Al Janaideh, S. Rakheja, and C.-Y. Su, "An analytical generalized prandtl-ishlinskii model inversion for hysteresis compensation in micropositioning control," *IEEE/ASME Trans. Mechatronics*, vol. 16, no. 4, pp. 734–744, Aug. 2011.

[91] G.-Y. Gu, M.-J. Yang, and L.-M. Zhu, "Real-time inverse hysteresis compensation of piezoelectric actuators with a modified prandtl-ishlinskii model," *Rev. Sci. Instrum.*, vol. 83, no. 6, pp. 065 106–1–8, 2012.

[92] M. Goldfarb and N. Celanovic, "Modeling piezoelectric stack actuators for control of micromanipulation," *IEEE Control Systems Magazine*, vol. 17, no. 3, pp. 69–79, Jun. 1997.

[93] M. Rakotondrabe, "Bouc-wen modeling and inverse multiplicative structure to compensate hysteresis nonlinearity in piezoelectric actuators," *IEEE Trans. Autom. Sci. Eng.*, vol. 8, no. 2, pp. 428–431, April 2011.

[94] Q. Xu and Y. Li, "Dahl model-based hysteresis compensation and precise positioning control of an XY parallel micromanipulator with piezoelectric actuation," *J. Dyn. Syst. Meas. Control-Trans. ASME*, vol. 132, no. 4, p. 041011, Jun. 2010.

[95] J. Kim and B. Kang, "Micro-macro linear piezoelectric motor based on self-moving cell," *Mechatronics*, vol. 19, no. 7, pp. 1134–1142, 2009.

[96] G.-Y. Gu, L.-M. Zhu, C.-Y. Su, H. Ding, and S. Fatikow, "Modeling and control of piezo-actuated nanopositioning stages: A survey," *IEEE Trans. Autom. Sci. Eng.*, no. 99, pp. 1–20, 2014.

[97] K. K. Leang and S. Devasia, "Design of hysteresis-compensating iterative learning control for piezo-positioners: Application to atomic force microscopes," *Mechatronics*, vol. 16, no. 3-4, pp. 141–158, Apr.-May 2006.

[98] J. Y. Peng and X. B. Chen, "Novel models for one-sided hysteresis of piezoelectric actuators," *Mechatronics*, vol. 22, no. 6, pp. 757–765, Sep. 2012.

[99] Q. Xu and P. K. Wong, "Hysteresis modeling and compensation of a piezostage using least squares support vector machines," *Mechatronics*, vol. 21, no. 7, pp. 1239–1251, 2011.

[100] M. S. Rana, H. R. Pota, I. R. Petersen, and H. Habibullah, "Nonlinearity compensation for improved nanopositioning of atomic force microscope," in *IEEE International Conference on Control Applications (CCA)*, Aug. 2013, pp. 461–466.

[101] N. Chuang, I. R. Petersen, and H. R. Pota, "Robust H^∞ control in fast atomic force microscopy," *Asian Journal of Control*, vol. 15, no. 3, pp. 872–887, May 2013.

[102] P.-L. Yen, M.-T. Yan, and Y. Chen, "Hysteresis compensation and adaptive controller design for a piezoceramic actuator system in atomic force microscopy," *Asian Journal of Control*, vol. 14, no. 4, pp. 1012–1027, July 2014.

[103] T. Zhanga, H. G. Li, and G. P. Cai, "Hysteresis identification and adaptive vibration control for a smart cantilever beam by a piezoelectric actuator," *Sensors and Actuators A: Physical*, vol. 203, p. 168, 2013.

[104] Y. S. Othman, I. A. Mahmood, A. M. Aibinu, and N. K. A. M. Rashid, "Frequency based hysteresis compensation for piezoelectric tube scanner using artificial neural networks," *Procedia Engineering*, vol. 41, pp. 757–763, 2012.

[105] J. W. Liang, H. Y. Chen, and S. Y. ; Chiang, "Precision control of a piezo-actuate system using fuzzy sliding-mode control with feedforward predictor-based compensation," *Materials Science Forum*, vol. 594, pp. 401–406, Nov. 2008.

[106] Y. Shan and K. K. Leang, "Dual-stage repetitive control with prandtl-ishlinskii hysteresis inversion for piezo-based nanopositioning," *Mechatronics*, vol. 22, no. 3, pp. 271–281, Apr. 2012.

[107] B. Kim, G. N. Washington, and H.-S. Yoon, "Hysteresis-reduced dynamic displacement control of piezoceramic stack actuators using model predictive sliding mode control," *Smart Materials and Structures*, vol. 21, no. 5, p. 055018, 2012.

[108] R. Comstock, "Charge control of piezoelectric actuators to reduce hysteresis effects," Apr. 1981, US Patent 4,263,527. [Online]. Available: http://www.google.com/patents/US4263527

[109] K. A. Yi and R. J. Veillette, "A charge controller for linear operation of a piezoelectric stack actuator," *IEEE Trans. Control Syst. Technol.*, vol. 13, no. 4, pp. 517–526, Jul. 2005.

[110] A. Fleming and S. Moheimani, "Improved current and charge amplifiers for driving piezoelectric loads, and issues in signal processing design for synthesis of shunt damping circuits," *J. Intell. Mater. Syst. Struct.*, vol. 15, pp. 77–92, 2004.

[111] G.-Y. Gu and L.-M. Zhu, "Comparative experiments regarding approaches to feedforward hysteresis compensation for piezoceramic actuators," *Smart Materials and Structures*, vol. 23, no. 9, p. 095029, 2014.

[112] G.-Y. Gu, L.-M. Zhu, C.-Y. Su, and H. Ding, "Motion control of piezoelectric positioning stages: Modeling, controller design, and experimental evaluation," *IEEE/ASME Trans. Mechatronics*, vol. 18, no. 5, pp. 1459–1471, Oct. 2013.

[113] Y. Liu, J. Shan, and U. Gabbert, "Feedback/feedforward control of hysteresis-compensated piezoelectric actuators for high-speed scanning applications," *Smart Materials and Structures*, vol. 24, no. 1, p. 015012, Nov. 2014.

[114] Y. Shan and K. Leang, "Design and control for high-speed nanopositioning: Serial-kinematic nanopositioners and repetitive control for nanofabrication," *IEEE Control Systems*, vol. 33, no. 6, pp. 86–105, Dec. 2013.

[115] B. Song, Z. Sun, N. Xi, R. Yang, and L. Chen, "High precision positioning control for SPM based nanomanipulation: A robust adaptive model reference control approach," in *IEEE/ASME International Conference on Advanced Intelligent Mechatronics (AIM)*, Jul. 2014, pp. 1658–1663.

[116] B. Mokaberi and A. Requicha, "Compensation of scanner creep and hysteresis for AFM nanomanipulation," *IEEE Trans. Autom. Sci. Eng.*, vol. 5, no. 2, pp. 197–206, April 2008.

[117] M. S. Rana, H. R. Pota, and I. R. Petersen, "Advanced control of atomic force microscope for faster image scanning," in *Applied Methods and Techniques for Mechatronic Systems*, ser. Lecture Notes in Control and Information Sciences, L. Liu et al., Ed. Springer Berlin Heidelberg, 2014, vol. 452, pp. 371–388.

[118] D. Croft, G. Shedd, and S. Devasia, "Creep, hysteresis, and vibration compensation for piezoactuators: atomic force microscopy application," *ASME Journal of Dynamic Systems, Measurement and Control*, vol. 123, no. 35, pp. 35–43, Mar. 2001.

[119] K. Kuhnen and P. Krejci, "Compensation of complex hysteresis and creep effects in piezoelectrically actuated systems - A new Preisach modeling approach," *IEEE Transactions on Automatic Control*, vol. 54, no. 3, pp. 537–550, Mar. 2009.

[120] K. K. Leang and S. Devasia, "Feedback-linearized inverse feedforward for creep, hysteresis, and vibration compensation in AFM piezoactuators," *IEEE Transactions on Control Systems Technology*, vol. 15, no. 5, pp. 927–935, Sep. 2007.

[121] C. Han and C. C. Chung, "Reconstruction of a scanned topographic image distorted by the creep effect of a Z scanner in atomic force microscopy," *Rev. Sci. Instrum.*, vol. 82, no. 5, pp. 053 709–053 709–9, May 2011.

[122] P. Krejci and K. Kuhnen, "Inverse control of systems with hysteresis and creep," *IEE Proceedings Control Theory and Applications*, vol. 148, no. 3, pp. 185–192, May 2001.

[123] M. S. Rana, H. R. Pota, and I. R. Petersen, "Nonlinearity effects reduction of an AFM piezoelectric tube scanner using MIMO MPC," *IEEE/ASME Trans. Mechatronics*, vol. 20, no. 3, pp. 1458–1469, Jun. 2015.

[124] B. Bhikkaji, Y. K. Yong, I. A. Mahmood, and S. Moheimani, "Multivariable control designs for piezoelectric tubes," in *Proceedings of the 18th IFAC World Congress*, Milano, Italy, Aug. 28Sep. 2 2011, pp. 2030–2035.

[125] M. Rakotondrabe, A. G. Fowler, and S. O. R. Moheimani, "Control of a novel 2-DOF MEMS nanopositioner with electrothermal actuation and sensing," *IEEE Trans. Control Syst. Technol.*, vol. 22, no. 4, pp. 1486–1497, Jul. 2014.

[126] M. W. Fairbairn, P. Muller, and S. Moheimani, "Sensorless implementation of a PPF controller for active q control of an AFM microcantilever," *IEEE Trans. Control Syst. Technol.*, vol. 22, no. 6, pp. 2118–2126, Nov. 2014.

[127] K. Karvinen and S. Moheimani, "Modulated-demodulated control: Q control of an AFM microcantilever," *Mechatronics*, vol. 24, no. 6, pp. 661–671, Sep. 2014.

[128] T. Sulchek, R. Hsieh, J. Adams, G. Yaralioglu, S. Minne, C. Quate, J. Cleveland, A. Atalar, and D. Adderton, "High-speed tapping mode imaging with active Q control for atomic force microscopy," *Applied Physics Letters*, vol. 76, no. 11, pp. 1473–1475, Mar. 2000.

[129] Y. Wu, Q. Zou, and C. Su, "A current cycle feedback iterative learning control approach for AFM imaging," *IEEE Trans. Nanotechnol.*, vol. 8, no. 4, pp. 515–527, Jul. 2009.

[130] K. S. Karvinen, M. Ruppert, K. Mahata, and S. O. R. Moheimani, "Direct tip-sample force estimation for high-speed dynamic mode atomic force microscopy," *IEEE Trans. Nanotechnol.*, vol. 13, no. 6, pp. 1257–1265, Nov. 2014.

[131] K. Chen, Y. Zhang, L. Beatrice, and R. Yang, "Stochastic noise tolerance: Enhanced full state observer vs. Kalman filter from video tracking perspective," *Journal of Electronics*, vol. 27, no. 4, pp. 557–563, Jul. 2010.

[132] A. E. Holman, P. M. L. O. Scholte, W. C. Heerens, and F. Tuinstra, "Analysis of piezo actuators in translation constructions," *Rev. Sci. Instrum.*, vol. 66, no. 5, pp. 3208–3215, 1995.

[133] M. S. Rana, H. R. Pota, and I. R. Petersen, "Spiral scanning with improved control for faster imaging of AFM," *IEEE Trans. Nanotechnol.*, vol. 13, no. 3, pp. 541–550, May 2014.

[134] C. L. Degen, U. Meier, Q. Lin, A. Hunkeler, and B. H. Meier, "Digital feedback controller for force microscope cantilevers," *Rev. Sci. Instrum.*, vol. 77, no. 4, pp. –, 2006. [Online]. Available: http://scitation.aip.org/content/aip/journal/rsi/77/4/10.1063/1.2183221

[135] S.-H. Hsu and L.-C. Fu, "Robust output high-gain feedback controllers for the atomic force microscope under high data sampling rate," in *Control Applications, 1999. Proceedings of the 1999 IEEE International Conference on*, vol. 2, 1999, pp. 1626–1631.

[136] I. A. Mahmood, S. O. R. Moheimani, and B. Bhikkaji, "A new scanning method for fast atomic force microscopy," *IEEE Transactions on Nanotechnology*, vol. 10, no. 2, pp. 203–216, Mar. 2011.

[137] A. Kotsopoulos, A. Pantazi, and T. Antonakopoulos, "Control for high-speed archimedean spiral nanopositioning," in *Proceedings of the 17th IEEE International Conference on Electronics, Circuits, and Systems (ICECS)*, Athens, Greece, Dec. 2010, pp. 998–1001.

[138] A. Kotsopoulos, A. Pantazi, A. Sebastian, and T. Antonakopoulos, "High-speed spiral nanopositioning," in *18th IFAC World Congress*, 2011, pp. 2018–2023.

[139] A. G. Kotsopoulos and T. A. Antonakopoulos, "Nanopositioning using the spiral of archimedes: The probe-based storage case," *Mechatronics*, vol. 20, no. 2, pp. 273–280, Mar. 2010.

[140] Y. K. Yong, S. O. R. Moheimani, and I. R. Petersen, "High-speed cycloid-scan atomic force microscopy," *Nanotechnology*, vol. 21, no. 36, pp. 365 503– 365 503–6, Sep. 2010.

[141] A. Bazaei, Y. K. Yong, and S. O. R. Moheimani, "High-speed lissajous-scan atomic force microscopy: Scan pattern planning and control design issues," *Rev. Sci. Instrum.*, vol. 83, no. 6, pp. 063 701–063 701–10, Jun. 2012.
[142] Y. Li and Q. Xu, "A totally decoupled piezo-driven XYZ flexure parallel micropositioning stage for micro/nanomanipulation," *IEEE Trans. Autom. Sci. Eng.*, vol. 8, no. 2, pp. 265–279, April 2011.
[143] B. J. Kenton and K. K. Leang, "Design and control of a three-axis serial-kinematic high-bandwidth nanopositioner," *IEEE/ASME Trans. Mechatronics*, vol. 17, no. 2, pp. 356–369, April 2012.
[144] Y. Li and Q. Xu, "Design and analysis of a totally decoupled flexure-based XY parallel micromanipulator," *IEEE Transactions on Robotics*, vol. 25, no. 3, pp. 645–657, Jun. 2009.
[145] A. G. Fowler, A. N. Laskovski, A. C. Hammond, and S. O. R. Moheimani, "A 2-DOF electrostatically actuated MEMS nanopositioner for on-chip AFM," *Journal of Microelectromechanical Systems*, vol. 21, no. 4, pp. 771–773, Aug. 2012.
[146] A. Mohammadi, A. G. Fowler, Y. K. Yong, and S. O. R. Moheimani, "A feedback controlled MEMS nanopositioner for on-chip high-speed AFM," *Journal of Microelectromechanical Systems*, vol. 23, no. 3, pp. 610–619, Jun. 2014.
[147] H. Watanabe, T. Uchihashi, T. Kobashi, M. Shibata, J. Nishiyama, R. Yasuda, and T. Ando, "Wide-area scanner for high-speed atomic force microscopy," *Rev. Sci. Instrum.*, vol. 84, no. 5, pp. 053 702–053 702–10, May 2013.
[148] Y. K. Yong, S. S. Aphale, and S. O. R. Moheimani, "Design, identification, and control of a flexure-based XY stage for fast nanoscale positioning," *IEEE Trans. Nanotechnol.*, vol. 8, no. 1, pp. 46–54, Jan. 2009.
[149] S. Wadikhaye, Y. Yong, and S. Moheimani, "Design of a compact serial-kinematic scanner for high-speed atomic force microscopy: An analytical approach," *Micro & Nano Letters, IET*, vol. 7, no. 4, pp. 309–313, Apr. 2012.
[150] Y. K. Yong, B. Bhikkaji, and S. O. Reza Moheimani, "Design, modeling, and FPAA-based control of a high-speed atomic force microscope nanopositioner," *IEEE/ASME Trans. Mechatronics*, vol. 18, no. 3, pp. 1060–1071, Jun. 2013.
[151] A. J. Fleming, "Dual-stage vertical feedback for high-speed scanning probe microscopy," *IEEE Trans. Control Syst. Technol.*, vol. 19, no. 1, pp. 156–165, Jan. 2011.
[152] K. K. Leang and A. J. Fleming, "High-speed serial-kinematic SPM scanner: design and drive considerations," *Asian Journal of Control*, vol. 11, no. 2, pp. 144–153, Mar. 2009.
[153] B. J. Kenton, A. J. Fleming, and K. K. Leang, "Compact ultra-fast vertical nanopositioner for improving scanning probe microscope scan speed," *Rev. Sci. Instrum.*, vol. 82, no. 12, pp. 123 703–123 703–8, Dec. 2011.
[154] G. M. Clayton, C. J. Dudley, and K. K. Leang, "Range-based control of dual-stage nanopositioning systems," *Rev. Sci. Instrum.*, vol. 85, no. 4, pp. 045 003–045 003–6, Apr. 2014.
[155] L. Petit, C. Prelle, E. Dore, F. Lamarque, and M. Bigerelle, "A four-discrete-position electromagnetic actuator: Modeling and experimentation," *IEEE/ASME Trans. Mechatronics*, vol. 15, no. 1, pp. 88–96, Feb. 2010.
[156] T. Tuma, W. Haeberle, H. Rothuizen, J. Lygeros, A. Pantazi, and A. Sebastian, "Dual-stage nanopositioning for high-speed scanning probe microscopy," *IEEE/ASME Trans. Mechatronics*, vol. 19, no. 3, pp. 1035–1045, Jun. 2014.
[157] J.-W. Wu, Y.-Z. Peng, J.-J. Chen, K.-C. Huang, M.-Y. Chen, and L.-C. Fu, "Design and implementation of a large measurement-range AFM scanning system," in *American Control Conference (ACC)*, Jun. 2012, pp. 895–900.
[158] C. Richter, P. Weinzierl, W. Engl, C. Penzkofer, B. Irmer, and T. Sulzbach, "Cantilever probes for high speed AFM," *Microsyst. Technol.*, vol. 18, no. 7-8, pp. 1119–1126, 2012.
[159] T. Ando, "High-speed atomic force microscopy coming of age," *Nanotechnology*, vol. 23, no. 6, pp. 062 001–062 001–27, 2012.
[160] M. Rakotondrabe, K. Rabenorosoa, J. Agnus, and N. Chaillet, "Robust feedforward-feedback control of a nonlinear and oscillating 2-DOF piezocantilever," *IEEE Trans. Autom. Sci. Eng.*, vol. 8, no. 3, pp. 506–519, July 2011.

M. S. Rana (S'12–M'15) was born in Bangladesh. He received a B.Sc. degree in electrical and electronic engineering from Rajshahi University of Engineering and Technology (RUET), Bangladesh, in 2008 and a Ph.D. in electrical engineering from the University of New South Wales (UNSW), Australia, in 2014.

He is currently an Assistant Professor in the Electrical and Electronic Engineering Department, RUET. He worked as a Research Associate and Visiting Fellow in the School of Engineering and Information Technology, UNSW, Australia. He also worked as a Lecturer in the Electrical and Electronic Engineering Department, University of Asia Pacific, Bangladesh. His research interests include control theory and applications, nanopositioning control, high-speed atomic force microscopy, mechatronics, and renewable energy integration.

Dr. Rana is a member of the Asian Control Association and the International Federation of Automatic Control. He received an award for Excellence in High Impact Journal Publications in 2014, from UNSW, Australia, as well as a Best Paper award at the 5th Australian Control Conference (AUCC), 2015.

H. R. Pota (M'13) received a B.E. degree from SVRCET, Surat, India, in 1979, a M.E. degree from the IISc, Bangalore, India, in 1981 and a Ph.D. from the University of Newcastle, NSW, Australia, in 1985, all in electrical engineering.

He is currently an Associate Professor at the University of New South Wales, Australian Defence Force Academy, Canberra, Australia. He has held visiting appointments at the University of Delaware; Iowa State University; Kansas State University; Old Dominion University; the University of California, San Diego; and the Centre for AI and Robotics, Bangalore. He has a continuing interest in the area of power system dynamics and control, and modeling & control of mechanical systems such as flexible structures, nanopositioning control, acoustical systems, and UAVs.

I. R. Petersen (F'99) was born in Victoria, Australia. He received a Ph.D. in electrical engineering in 1984 from the University of Rochester, Rochester, NY, USA. From 1983 to 1985, he was a Postdoctoral Fellow at the Australian National University. In 1985, he joined the University of New South Wales, Canberra, Australia, where he is currently a Scientia Professor and an Australian Research Council Laureate Fellow in the School of Engineering and Information Technology. His main research interests are in robust control theory, quantum control theory, and stochastic control theory.

Dr. Petersen has served as an Associate Editor for the IEEE Transactions on Automatic Control, Systems and Control Letters, Automatica, and SIAM Journal on Control and Optimization. He is currently an Editor for Automatica. He is a fellow of IFAC, the IEEE and the Australian Academy of Science.